Bachelor's thesis

Deep Inelastic $e^{\pm}p$ Scattering with Boson Exchange and Interference

Tiefinelastische Streuung mit Vektor-Boson-Austausch und -Interferenz

Carlson M. Büth

Working group Klasen

Supervisor and first examiner: Priv.-Doz. Dr. Karol Kovařík
Second examiner: Prof. Dr. Michael Klasen

Institute of Theoretical Physics
University of Münster, Germany

Münster, September 15, 2020

Contents

1. Introduction

With every advance in technology, accelerators could produce higher and higher beam energies. Hofstadter and collaborators observed in the 1960s, that the proton has a finite radius of approximately 10^{-13} cm and behaves not exactly as a point charge. This was discovered when examining a scattering cross section. Early experiments at the Stanford Linear Accelerator Center (SLAC) carried out by MIT physicists, researched elastic electron-proton scattering with excitation energies up to less than 2 GeV [Ken91]. To look for higher resonances and in order to reach the inelastic continuum, the accelerator was upgraded to 20 GeV a decade later. Without expecting it, a weak q^2 dependence was found and secondly scaling as suggested by Bjorken in 1968 [Fri91]. Nowadays energies of scattering experiments can be over four orders of magnitude larger [Hou+19]. But already at energies with one order of magnitude more, previous mathematical models deduced using SLAC data, are not sufficient.

This bachelor's thesis aims to describe $e^{\pm}p$ scattering on a parton level, including the exchange and interference of γ, Z, and $W^{\pm}$ vector bosons. From the detailed calculation of Feynman diagrams to an implementation of a function that process patron density functions (PDFs) into a cross section. The theoretical prediction will be compared to measurements of the scattering data. This is done with combined HERA data at 920 GeV ($\sqrt{2} = 318$ GeV) which is claimed to be "the most precise data due to the large integrated luminosity" [Hou+19, p. 29]. A further goal of the thesis is to show how PDFs evolved in the past 20 years. We will analyze three CTEQ PDFs: CTEQ6 (2002), CT10 (2010) and CT18NNLO (2019) [Pum+02; Lai+10; Hou+19].

2. Preliminaries

To understand electron-proton scattering, it is instructive to consider the underlying interactions with the quark content. To prepare for this, we will review electron-muon scattering first, because it is fairly similar to the quark interaction. After this, we'll apply it to the quark interaction.

2.1. Electron-Muon Scattering

$e^-\mu^- \to e^-\mu^-$ scattering proceeds via the t-channel neutral current exchange. Vector boson γ carries the electromagnetic interaction and Z the electroweak. At tree level the two diagrams Figs. 1 and 2 are the only ones for this reaction. The Feynman rules used here are given in Appendix A.4.[1][2]

2.1.1. γ^* exchange

First is the Feynman diagram displayed in Fig. 1. A virtual photon γ^* is the exchange particle here. Feynman rules for $-i\mathcal{M}$ give the invariant amplitude

$$-i\mathcal{M}_\gamma = \overline{u}(p_B)(ie)\gamma^\mu u(p_A) \cdot \frac{-ig_{\mu\nu}}{(p_A - p_B)^2} \cdot \overline{u}(k_2)(ie)\gamma^\nu u(k_1), \quad (2.1)$$

$$\mathcal{M}_\gamma = \frac{-e^2}{t} \cdot \overline{u}(p_B)\gamma^\mu u(p_A) \cdot \overline{u}(k_2)\gamma_\mu u(k_1), \quad (2.2)$$

where t is a Mandelstam variable $t = (p_A - p_B)^2$. For unpolarized cross section, we have to sum (and average) over spins

$$\overline{|\mathcal{M}_\gamma|^2} = \frac{1}{2}\sum_{e^-\text{spins}} \frac{1}{2}\sum_{\mu^-\text{spins}} \mathcal{M}_\gamma \mathcal{M}_\gamma^\dagger = \frac{e^4}{t^2} L_{e^-}^{\mu\nu} L_{\mu\nu}^{\mu^-}, \quad (2.3)$$

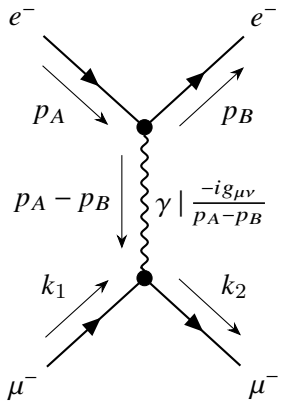

Figure 1: Electromagnetic electron-muon scattering in lowest order.

where

$$L_{e^-}^{\mu\nu} = \frac{1}{2}\sum_{e^-\text{spins}} [\overline{u}(p_B)\gamma^\mu u(p_A)] \underbrace{[\overline{u}(p_B)\gamma^\nu u(p_A)]^*}_{=[\overline{u}(p_A)\gamma^\nu u(p_B)]}. \quad (2.4)$$

using $[\overline{u}(p_B)\gamma^\nu u(p_A)]^* = \left[u^\dagger(p_B)\gamma^0\gamma^\nu u(p_A)\right]^\dagger = u^\dagger(p_A)\gamma^{\nu\dagger}\gamma^0 u(p_B) = \overline{u}(p_A)\gamma^\nu u(p_B)$ (using $\gamma^{\nu\dagger}\gamma^0 = \gamma^0\gamma^\nu$). Analogously

$$L_{\mu\nu}^{\mu^-} = \frac{1}{2}\sum_{\mu^-\text{spins}} \left[\overline{u}(k_2)\gamma_\mu u(k_1)\right] \underbrace{[\overline{u}(k_2)\gamma_\nu u(k_1)]^*}_{=[\overline{u}(k_1)\gamma_\nu u(k_2)]}. \quad (2.5)$$

[1] Ell17, Diagrams are drawn with Ti*k*Z-Feynman unless otherwise stated.
[2] SMO20, All calculations presented here were checked against calculations with FeynCalc.

When rearranging the leptonic tensors L, the completeness relation Eq. (A.11) for a fermion can be used. To advance there is a need for trace theorems as seen in Appendix A.2.

$$\begin{aligned}
L_{e^-}^{\mu\nu} &= \frac{1}{2}\sum_{s_2}\overline{u}_\alpha^{(s_2)}(p_B)\gamma^\mu_{\alpha\beta}\sum_{s_2}u_\beta^{(s_1)}(p_B)\overline{u}_\gamma^{(s_1)}(p_A)\gamma^\nu_{\gamma\delta}u_\delta^{(s_2)}(p_B)\\
&= \frac{1}{2}\underbrace{\sum_{s_2}u_\delta^{(s_2)}(p_B)\overline{u}_\alpha^{(s_2)}(p_B)}_{(\not{p}_B+m_e)_{\delta\alpha}}\gamma^\mu_{\alpha\beta}\underbrace{\sum_{s_2}u_\beta^{(s_1)}(p_B)\overline{u}_\gamma^{(s_1)}(p_A)}_{(\not{p}_A+m_e)_{\beta\gamma}}\gamma^\nu_{\gamma\delta}\\
&= \frac{1}{2}\operatorname{Tr}\left[(\not{p}_B+m_e)_{\delta\alpha}\gamma^\mu_{\alpha\beta}(\not{p}_A+m_e)_{\beta\gamma}\gamma^\nu_{\gamma\delta}\right]\\
&= \frac{1}{2}\operatorname{Tr}\left(\not{p}_B\gamma^\mu\not{p}_A\gamma^\nu\right)+\frac{1}{2}m_e^2\operatorname{Tr}\left(\gamma^\mu\gamma^\nu\right) = 2\left(p_B^\mu p_A^\nu + p_B^\nu p_A^\mu - \left(p_B\cdot p_A - m_e^2\right)g^{\mu\nu}\right) \qquad (2.6)\\
L_{\mu\nu}^{\mu^-} &= \frac{1}{2}(\not{k}_2+m_\mu)^{\delta\alpha}\gamma_\mu^{\alpha\beta}(\not{k}_1+m_\mu)^{\beta\gamma}\gamma_\nu^{\gamma\delta} = \frac{1}{2}\operatorname{Tr}\left[(\not{k}_2+m_\mu)^{\delta\alpha}\gamma_\mu^{\alpha\beta}(\not{k}_1+m_\mu)^{\beta\gamma}\gamma_\nu^{\gamma\delta}\right]\\
&= 2\left(k_{2,\mu}k_{1,\nu}+k_{2,\nu}k_{1,\mu}-\left(k_2\cdot k_1-m_\mu^2\right)g_{\mu\nu}\right) \qquad (2.7)
\end{aligned}$$

Combining leads to

$$\overline{|\mathcal{M}|^2} = \frac{e^4}{t^2}L_{e^-}^{\mu\nu}L_{\mu\nu}^{\mu^-} = \frac{8e^4}{t^2}\Big((p_B\cdot k_2)(p_A\cdot k_1)+(p_B\cdot k_1)(p_A\cdot k_2)\underbrace{-m_e^2k_2\cdot k_1-m_\mu^2p_B\cdot p_A+2m_e^2m_\mu^2}_{\text{in the massless limit }=0}\Big). \qquad (2.8)$$

This is also expressible through the Mandelstam variables:

$$\begin{aligned}
\overline{|\mathcal{M}|^2} &= \frac{32e^2}{t^2}\left[(s-m_e^2-m_\mu^2)^2+(m_e^2+m_\mu^2-u)^2+2(m_e^2+m_\mu^2)t\right] \qquad (2.9)\\
&\overset{s,u,t\gg m_e,m_\mu}{=} 2e^4\frac{s^2+u^2}{t^2} \qquad (2.10)
\end{aligned}$$

2.1.2. Z^0 exchange

Secondly comes the Feynman diagram with the electroweak interaction of the electrically neutral vector Z^0 boson. For this diagram a new propagator as given in Fig. 2 is needed as well as a new vertex factor

$$ie\gamma^\mu \to -i\frac{g}{\cos\theta_W}\gamma^\mu\frac{1}{2}(g_V^f-a_V^f\gamma^5) \qquad (2.11)$$

where $g\sin\theta_W = e$, and g_V^f, a_V^f constant vertex factors for a fermion f. For the electron and muon they are equal

$$a_V^{e,\mu} = -\frac{1}{2} \qquad \text{and} \qquad g_V^{e,\mu} = -\frac{1}{2}+\sin^2\theta_W. \qquad (2.12)$$

θ_W is called the Weinberg or weak mixing angle.

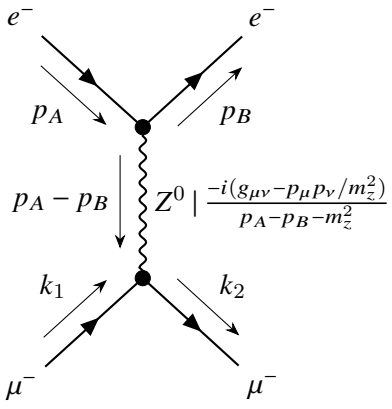

Figure 2: Electroweak electron-muon scattering in lowest order.

Using $g_V = C_L + C_R$ and $a_V = C_L - C_R$ the vertex factor can be rewritten as

$$\frac{1}{2}\left(g_V - a_V\gamma^5\right) = \frac{1}{2}\left(C_L + C_R - (C_L - C_R)\,\gamma^5\right) = C_L\frac{1}{2}\left(1-\gamma^5\right) + C_R\frac{1}{2}\left(1+\gamma^5\right) = C_L P_L + C_R P_R. \tag{2.13}$$

The operators P_L and P_R are called the chiral projection operators and span an orthonormal system for the helicity of particles. More on that in Appendix A.3. The Lorentz invariant amplitude is given using the Feynman Rules for the diagram in Fig. 2.[3]

$$\begin{aligned} -i\mathcal{M}_Z =& \overline{u}(p_B)\frac{-ig}{c_W}\gamma^\mu\left(C_L^e P_L + C_R^e P_R\right)u(p_A)\cdot(-i)\frac{g_{\mu\nu} - \frac{p_\mu p_\nu}{m_Z^2}}{t - m_Z^2} \\ &\cdot \overline{u}(k_2)\frac{-ig}{c_W}\gamma^\nu\left(C_L^\mu P_L + C_R^\mu P_R\right)u(k_1) \end{aligned} \tag{2.14}$$

$$\begin{aligned} \mathcal{M}_Z =& -\frac{g^2}{4c_W^2}\left[\overline{u}(p_B)\gamma^\mu\left(C_L^e P_L + C_R^e P_R\right)u(p_A)\right]\cdot\left(\frac{g_{\mu\nu} - \frac{p_\mu p_\nu}{m_Z^2}}{t - m_Z^2}\right) \\ &\cdot\left[\overline{u}(k_2)\gamma^\nu\left(C_L^\mu P_L + C_R^\mu P_R\right)u(k_1)\right] \end{aligned} \tag{2.15}$$

where m_Z is the mass of the Z boson. The mass is much bigger than the mass of the colliding particles and so $\frac{p_\mu p_\nu}{m_Z^2}$ does not contribute: $m_Z \gg m_e, m_\mu \Rightarrow \frac{1}{2}(p_A - p_B)_\sigma\,\overline{u}(p_B)\gamma^\sigma u(p_A) = 0 \Rightarrow g_{\mu\nu} - \frac{p_\mu p_\nu}{m_Z^2} = g_{\mu\nu}$

$$\mathcal{M}_Z = -\frac{g^2}{c_W^2}\left[\overline{u}(p_B)\gamma^\mu\left(C_L^e P_L + C_R^e P_R\right)u(p_A)\right]\frac{g_{\mu\nu}}{t - m_Z^2}\left[\overline{u}(k_2)\gamma^\nu\left(C_L^\mu P_L + C_R^\mu P_R\right)u(k_1)\right] \tag{2.16}$$

$$\mathcal{M}_Z^\dagger = -\frac{g^2}{c_W^2}\left[\overline{u}(p_A)\gamma^\mu\left(C_L^e P_L + C_R^e P_R\right)u(p_B)\right]\frac{g_{\mu\nu}}{t - m_Z^2}\left[\overline{u}(k_1)\gamma^\nu\left(C_L^\mu P_L + C_R^\mu P_R\right)u(k_2)\right] \tag{2.17}$$

These simple forms are again possible because of the hermitian conjugate of the transition matrix:

$$\begin{aligned} \left[\overline{u}(p_B)\gamma^\mu\left(C_L^e P_L + C_R^e P_R\right)u(p_A)\right]^* &= \left[u^\dagger(p_B)\gamma^0\gamma^\mu\frac{1}{2}\left(g_V^e - a_V^e\gamma^5\right)u(p_A)\right]^\dagger \\ &= u^\dagger(p_A)\left(g_V^e - a_V^e\gamma^{5\dagger}\right)\frac{1}{2}\gamma^{\mu\dagger}\gamma^0 u(p_B) \\ \gamma^{\mu\dagger}\gamma^0 = \gamma^0\gamma^\mu \Rightarrow &= u^\dagger(p_A)\frac{1}{2}\left(g_V^e - a_V^e\gamma^{5\dagger}\right)\gamma^0\gamma^\mu u(p_B) \\ &= u^\dagger(p_A)\gamma^0\frac{1}{2}\left(g_V^e + a_V^e\gamma^{5\dagger}\right)\gamma^\mu u(p_B) \\ \left\{\gamma^\xi, \gamma^5\right\} = 0 \Rightarrow &= \overline{u}(p_A)\gamma^\mu\frac{1}{2}\left(g_V^e - a_V^e\gamma^5\right)u(p_B) \\ &= \left[\overline{u}(p_A)\gamma^\mu\left(C_L^e P_L + C_R^e P_R\right)u(p_B)\right] \end{aligned} \tag{2.18}$$

The calculation is analogous to the previous diagram:

$$\overline{|\mathcal{M}_Z|^2} = \frac{g^4}{c_W^4}\frac{1}{\left(t - m_Z^2\right)^2}\cdot\sum_{\text{spins}}\left[\overline{u}(p_B)\gamma^\mu\left(C_L^e P_L + C_R^e P_R\right)u(p_A)\right]g_{\mu\nu}\left[\overline{u}(k_2)\gamma^\nu\left(C_L^\mu P_L + C_R^\mu P_R\right)u(k_1)\right]$$

[3] From here on we use shorthands s_W and c_W for $\sin\theta_W$ and $\cos\theta_W$.

$$\cdot \left[\overline{u}(p_A)\gamma^\alpha \left(C_L^e P_L + C_R^e P_R\right) u(p_B)\right] g_{\alpha\beta} \left[\overline{u}(k_1)\gamma^\beta \left(C_L^\mu P_L + C_R^\mu P_R\right) u(k_2)\right] \tag{2.19}$$

First, sort the spin sums pairwise and apply the completeness relation.

$$\begin{aligned}
\overline{|\mathcal{M}_Z|^2} =& \frac{g^4}{c_W^4} \frac{1}{\left(t - m_Z^2\right)^2} \left(\frac{1}{2} \sum_{e^-\text{-spins}} \overline{u}(p_B)\gamma^\mu \left(C_L^e P_L + C_R^e P_R\right) u(p_A)\overline{u}(p_A)\gamma^\alpha \left(C_L^e P_L + C_R^e P_R\right) u(p_B)\right) \times \\
& \left(\frac{1}{2} \sum_{e^\mu\text{-spins}} \overline{u}(k_2)\gamma^\nu \left(C_L^\mu P_L + C_R^\mu P_R\right) u(k_1)\overline{u}(k_1)\gamma^\beta \left(C_L^\mu P_L + C_R^\mu P_R\right) u(k_2)\right) g_{\mu\nu} g_{\alpha\beta} \qquad (2.20) \\
=& \frac{g^4}{4c_W^4} \frac{1}{\left(t - m_Z^2\right)^2} \left(\sum_{e^-\text{-spins}} u(p_B)\overline{u}(p_B)\gamma^\mu \frac{1}{2}\left(g_V^e - a_V^e\gamma^5\right) u(p_A)\overline{u}(p_A)\gamma^\alpha \frac{1}{2}\left(g_V^e - a_V^e\gamma^5\right)\right) \times \\
& \left(\sum_{e^\mu\text{-spins}} u(k_2)\overline{u}(k_2)\gamma^\nu \frac{1}{2}\left(g_V^\mu - a_V^\mu\gamma^5\right) u(k_1)\overline{u}(k_1)\gamma^\beta \frac{1}{2}\left(g_V^\mu - a_V^\mu\gamma^5\right)\right) g_{\mu\nu} g_{\alpha\beta} \qquad (2.21) \\
=& \frac{g^4}{16c_W^4} \frac{1}{\left(t - m_Z^2\right)^2} \operatorname{Tr}\left[\left(\not{p}_B + m_e\right)\gamma^\mu \left(g_V^e - a_V^e\gamma^5\right)\left(\not{p}_A + m_e\right)\gamma^\alpha \left(g_V^e - a_V^e\gamma^5\right)\right] \\
& \cdot \operatorname{Tr}\left[\left(\not{k}_2 + m_\mu\right)\gamma^\nu \left(g_V^\mu - a_V^\mu\gamma^5\right)\left(\not{k}_1 + m_\mu\right)\gamma^\beta \left(g_V^\mu - a_V^\mu\gamma^5\right)\right] g_{\mu\nu} g_{\alpha\beta} \qquad (2.22)
\end{aligned}$$

To streamline, we solve again the traces in the massless limit $m_e, m_\mu = 0$ with the diverse trace theorems of Appendix A.2.

$$\begin{aligned}
\operatorname{Tr}_1[...] =& \operatorname{Tr}\left[\not{p}_B\gamma^\mu \left(g_V^e - a_V^e\gamma^5\right)\not{p}_A\gamma^\alpha \left(g_V^e - a_V^e\gamma^5\right)\right] \\
=& (g_V^e)^2 \operatorname{Tr}\left[\not{p}_B\gamma^\mu\not{p}_A\gamma^\alpha\right] - g_V^e a_V^e \operatorname{Tr}\left[\not{p}_B\gamma^\mu\not{p}_A\gamma^\alpha\gamma^5\right] \\
& - a_V^e g_V^e \operatorname{Tr}\left[\not{p}_B\gamma^\mu\gamma^5\not{p}_A\gamma^\alpha\right] + (a_V^e)^2 \operatorname{Tr}\left[\not{p}_B\gamma^\mu\gamma^5\not{p}_A\gamma^\alpha\gamma^5\right] \\
=& (g_V^e)^2 \operatorname{Tr}\left[\not{p}_B\gamma^\mu\not{p}_A\gamma^\alpha\right] - 2g_V^e a_V^e \operatorname{Tr}\left[\not{p}_B\gamma^\mu\not{p}_A\gamma^\alpha\gamma^5\right] + (a_V^e)^2 \mathrm{tr}[\not{p}_B\gamma^\mu\not{p}_A\gamma^\alpha \underbrace{\gamma^5\gamma^5}_{=\mathbb{1}}] \\
=& \left((g_V^e)^2 + (a_V^e)^2\right) \operatorname{Tr}\left[\not{p}_B\gamma^\mu\not{p}_A\gamma^\alpha\right] - 2g_V^e a_V^e \operatorname{Tr}\left[\not{p}_B\gamma^\mu\not{p}_A\gamma^\alpha\gamma^5\right] \\
=& \left((g_V^e)^2 + (a_V^e)^2\right) 4\left(p_A^\alpha p_B^\mu + p_A^\mu p_B^\alpha - (p_A p_B)\, g^{\mu\alpha}\right) - 2g_V^e a_V^e p_{B,\delta} p_{A,\gamma} (-4i)\epsilon^{\delta\mu\gamma\alpha}
\end{aligned} \tag{2.23}$$

Similarly

$$\operatorname{Tr}_2[...] = \left((g_V^\mu)^2 + (a_V^\mu)^2\right) 4\left(k_{1,\beta}k_{2,\nu} + k_{1,\nu}k_{2,\beta} - (k_1 k_2)\, g_{\nu\beta}\right) - 2g_V^\mu a_V^\mu k_2^{\not{}} k_1^{\not{}} (-4i)\epsilon_{\not{}\nu\not{}\beta}. \tag{2.24}$$

With the last identity of Eq. (A.6), combining theses gives

$$\begin{aligned}
\operatorname{Tr}_1[...] \operatorname{Tr}_2[...] g_{\mu\nu} g_{\alpha\beta} =& 16\left((g_V^e)^2 + (a_V^e)^2\right)\left((g_V^\mu)^2 + (a_V^\mu)^2\right)\left(2\,(p_A k_1)\,(p_B k_2) + 2\,(p_A k_2)\,(p_B k_1)\right. \\
& \left. - 2\,(p_A p_B)\,(k_1 k_2) - 2\,(k_1 k_2)\,(p_A p_B) + 4\,(p_A p_B)\,(k_1 k_2)\right) \\
& + 32i\left((g_V^e)^2 + (a_V^e)^2\right) g_V^\mu a_V^\mu \underbrace{\left(p_A^\nu p_B^\beta + p_A\beta p_B^\nu\right) k_2^{\not{}} k_1^{\not{}} \epsilon_{\not{}\nu\not{}\beta}}_{=0 \text{ because } \epsilon_{\not{}\nu\not{}\beta} = -\epsilon_{\not{}\beta\not{}\nu}}
\end{aligned}$$

$$
\begin{aligned}
&+ 32ig_V^e a_V^e \left((g_V^\mu)^2 + (a_V^\mu)^2\right) p_{B,\delta} p_{A,\gamma} \underbrace{\left(k_{1,\mu} k_{2,\alpha} + k_{1,\alpha} k_{2,\mu}\right) \epsilon^{\delta\mu\gamma\alpha}}_{=0} \\
&- 64 g_V^e a_V^e g_V^\mu a_V^\mu p_{B,\delta} p_{A,\gamma} k_2^{\blacktriangleleft} k_1^{\blacktriangleright} \underbrace{\epsilon^{\delta\mu\gamma\alpha} \epsilon_{\blacktriangleleft\mu\blacktriangleright\alpha}}_{-2\left(\delta^\delta_{\blacktriangleleft}\delta^\gamma_{\blacktriangleright} - \delta^\delta_{\blacktriangleright}\delta^\gamma_{\blacktriangleleft}\right)} \qquad (2.25) \\
&= 32 \left((g_V^e)^2 + (a_V^e)^2\right) \left((g_V^\mu)^2 + (a_V^\mu)^2\right) \left((p_A k_1)(p_B k_2) + (p_A k_2)(p_B k_1)\right) \qquad (2.26) \\
&+ 128 g_V^e a_V^e g_V^\mu a_V^\mu p_{B,\delta} p_{A,\gamma} k_2^{\blacktriangleleft} k_1^{\blacktriangleright} \left(\delta^\delta_{\blacktriangleleft}\delta^\gamma_{\blacktriangleright} - \delta^\delta_{\blacktriangleright}\delta^\gamma_{\blacktriangleleft}\right).
\end{aligned}
$$

When using the 4-momentum conservation with neglected masses $p_A + k_1 = p_B + k_2 \Rightarrow p_A \cdot k_1 = p_B \cdot k_2$. For the Mandelstam variables $s = (p_A + k_1)^2 \simeq 2p_A \cdot k_1$ and $u = (p_A + k_2)^2 \simeq 2p_A \cdot k_2 = 2p_B \cdot k_1$. Then the formula reduces to

$$
\mathrm{Tr}_1[...]\,\mathrm{Tr}_2[...] g_{\mu\nu} g_{\alpha\beta} = 2\left((g_V^e)^2 + (a_V^e)^2\right)\left((g_V^\mu)^2 + (a_V^\mu)^2\right)\left(s^2 + u^2\right) + 8 g_V^e g_V^\mu a_V^e a_V^\mu \left(s^2 - u^2\right) \qquad (2.27)
$$

and the squared (averaged) matrix element is

$$
\overline{|\mathcal{M}_Z|^2} = \frac{e^4}{8 c_W^4 s_W^4} \frac{1}{\left(t - m_Z^2\right)^2} \left[\left((g_V^e)^2 + (a_V^e)^2\right)\left((g_V^\mu)^2 + (a_V^\mu)^2\right)\left(s^2 + u^2\right) + 4 g_V^e g_V^\mu a_V^e a_V^\mu \left(s^2 - u^2\right)\right]. \qquad (2.28)
$$

2.1.3. Interference

For the full invariant amplitude $\overline{|\mathcal{M}|^2} = \frac{1}{2}\sum_{\text{spin}} \left\{|\mathcal{M}_\gamma|^2 + |\mathcal{M}_Z|^2 + 2\Re\left(\mathcal{M}_\gamma \mathcal{M}_Z^\dagger\right)\right\}$ there is a interference term needed. Let's calculate it in the following. First a recap of the amplitudes:

$$
\mathcal{M}_\gamma = \overline{u}(p_B)(ie)\gamma^\mu u(p_A) \frac{-g_{\mu\nu}}{(p_A - p_B)^2} \overline{u}(k_2)(ie)\gamma^\nu u(k_1) \qquad (2.29)
$$

$$
\mathcal{M}_Z = \overline{u}(p_B)\left(\frac{-ig}{\cos\theta_W}\right)\gamma^\mu \left[C_L^e P_L + C_R^e P_R\right] u(p_A) \frac{-g_{\mu\nu} + \frac{p_\mu p_\nu}{m_Z^2}}{t - m_Z^2} \overline{u}(k_2)\left(\frac{-ig}{\cos\theta_W}\right)\gamma^\nu \left[C_L^\mu P_L + C_R^\mu P_R\right] u(k_1) \qquad (2.30)
$$

$$
\mathcal{M}_Z^\dagger = \overline{u}(p_A)\left(\frac{ig}{\cos\theta_W}\right)\gamma^\mu \left[C_L^e P_L + C_R^e P_R\right] u(p_B) \frac{-g_{\mu\nu} + \frac{p_\mu p_\nu}{m_Z^2}}{t - m_Z^2} \overline{u}(k_1)\left(\frac{ig}{\cos\theta_W}\right)\gamma^\nu \left[C_L^\mu P_L + C_R^\mu P_R\right] u(k_2). \qquad (2.31)
$$

Now the amplitudes have to be combined, as

$$
\begin{aligned}
&\sum_{\text{spin}} \Re\Bigg[\left(\overline{u}(p_B)(ie)\gamma^\mu u(p_A) \frac{-g_{\mu\nu}}{t} \overline{u}(k_2)(ie)\gamma^\nu u(k_1)\right) \times \qquad (2.32) \\
&\left(\overline{u}(p_A)\left(\frac{ig}{\cos\theta_W}\right)\gamma^\alpha \left[C_L^e P_L + C_R^e P_R\right] u(p_B) \frac{-g_{\alpha\beta} + \frac{p_\alpha p_\beta}{m_Z^2}}{t - m_Z^2} \overline{u}(k_1)\left(\frac{ig}{\cos\theta_W}\right)\gamma^\beta \left[C_L^\mu P_L + C_R^\mu P_R\right] u(k_2)\right)\Bigg]
\end{aligned}
$$

Previous steps are now repeated neglecting the contribution from the $\frac{p_\mu p_\nu}{m_Z^2}$ term.

$$\frac{1}{2}\sum_{\text{spin}} 2\Re\left(\mathcal{M}_\gamma \mathcal{M}_Z^\dagger\right) = \frac{g^2}{\cos^2\theta_W}\frac{1}{t\left(t-m_Z^2\right)}\Re\Bigg[\left(\sum_{e\text{-spin}} \overline{u}(p_B)\gamma^\mu u(p_A)\overline{u}(p_A)\gamma^\alpha\left[C_L^e P_L + C_R^e P_R\right]u(p_B)\right)\times \left(\sum_{\mu\text{-spin}} \overline{u}(k_2)\gamma^\nu u(k_1)\overline{u}(k_1)\gamma^\beta\left[C_L^\mu P_L + C_R^\mu P_R\right]u(k_2)\right) g_{\mu\nu}g_{\alpha\beta}\Bigg] \tag{2.33}$$

$$= \frac{g^2}{\cos^2\theta_W}\frac{1}{t\left(t-m_Z^2\right)}\Re\Bigg[\operatorname{Tr}\left[\left(\not{p}_B + m_e\right)\gamma^\mu\left(\not{p}_A + m_e\right)\gamma^\alpha\left[C_L^e P_L + C_R^e P_R\right]\right]\times \operatorname{Tr}\left[\left(\not{k}_2 + m_\mu\right)\gamma^\nu\left(\not{k}_1 + m_\mu\right)\gamma^\beta\left[C_L^\mu P_L + C_R^\mu P_R\right]\right] g_{\mu\nu}g_{\alpha\beta}\Bigg] \tag{2.34}$$

Determining the traces in the limit $m_e, m_\mu \to 0$ gives

$$\operatorname{Tr}\left[\not{p}_B\gamma^\mu\not{p}_A\gamma^\alpha\left[C_L^e\frac{1}{2}\left(1-\gamma^5\right) + C_R^e\frac{1}{2}\left(1+\gamma^5\right)\right]\right] \tag{2.35}$$

$$= \operatorname{Tr}\left[\not{p}_B\gamma^\mu\not{p}_A\right]\frac{1}{2}\underbrace{\left(C_L^e + C_R^e\right)}_{g_V^e} + \frac{1}{2}\underbrace{\left(C_L^e - C_R^e\right)}_{a_V^e}\operatorname{Tr}\left[\not{p}_B\gamma^\mu\not{p}_A\gamma^5\right] \tag{2.36}$$

$$= \frac{1}{2}g_V^e 4\left(p_A^\alpha p_B^\beta + p_A^\beta p_B^\alpha - \left(p_A p_B\right)g^{\mu\alpha}\right) - \frac{1}{2}a_V^e p_{B,\beta}p_{A,\nu}(-4i)\epsilon^{\beta\mu\alpha\nu}, \tag{2.37}$$

$$\operatorname{Tr}_2\left[\ldots\right] = \frac{1}{2}g_V^\mu 4\left(k_{1,\alpha}k_{2,\beta} + k_{1,\beta}k_{2,\alpha} - \left(k_1 k_2\right)g_{\mu\alpha}\right) + 2ia_V^e k_2^\beta k_1^\nu \epsilon_{\beta\mu\alpha\nu}. \tag{2.38}$$

Together they are

$$\operatorname{Tr}_1\left[\ldots\right]\operatorname{Tr}_2\left[\ldots\right] = 4g_V^e g_V^\mu\Big(2\left(p_A k_1\right)\left(p_B k_2\right) + 2\left(p_A k_2\right)\left(p_B k_1\right) - 2\left(p_A p_B\right)\left(k_1 k_2\right) - 2\left(k_1 k_2\right)\left(p_A p_B\right) + 4\left(p_A p_B\right)\left(k_1 k_2\right)\Big) - 4a_V^e a_V^\mu p_{B,\beta}p_{A,\nu}k_2^\delta k_1^\eta \epsilon^{\beta\mu\alpha\nu}\epsilon_{\delta\mu\eta\nu} \tag{2.39}$$

$$= 8\left(g_V^e g_V^\mu\left(\left(p_A k_1\right)\left(p_B k_2\right) + \left(p_A k_2\right)\left(p_B k_1\right)\right) + a_V^e a_V^\mu p_{B,\beta}p_{A,\nu}k_2^\delta k_1^\eta\left(\delta_\delta^\beta\delta_\eta^\alpha - \delta_\eta^\beta\delta_\delta^\alpha\right)\right). \tag{2.40}$$

Neglecting the masses again $p_A + k_1 = p_B + k_2$ turns to $p_A k_1 = p_B k_2$ and then with Mandelstam variables the solution is

$$\sum_{\text{spin}}\Re\left(\mathcal{M}_\gamma\mathcal{M}_Z^\dagger\right) = \frac{e^4}{2c_W^2 s_W^2}\frac{1}{t\left(t-m_Z^2\right)}\Big(-2g_V^e g_V^\mu\left(\left(p_A k_1\right)\left(p_B k_2\right) + \left(p_A k_2\right)\left(p_B k_1\right)\right) + 2a_V^e a_V^\mu\left(\left(p_A k_2\right)\left(p_B k_1\right) - \left(p_A k_1\right)\left(p_B k_2\right)\right)\Big) \tag{2.41}$$

$$= \frac{e^4}{2c_W^2 s_W^2}\frac{1}{t\left(t-m_Z^2\right)}\left(-2g_V^e g_V^\mu\left(s^2+u^2\right) - 2a_V^e a_V^\mu\left(s^2-u^2\right)\right). \tag{2.42}$$

(a) Electromagnetic. (b) Electroweak.

Figure 3: $e^-q \to e^-q$ scattering in lowest order.

2.1.4. Final result

Adding all contributions the full invariant amplitude is $\overline{|\mathcal{M}|^2} = \overline{|\mathcal{M}_\gamma|^2} + \overline{|\mathcal{M}_Z|^2} + \sum_{\text{spin}} \Re\left(\mathcal{M}_\gamma \mathcal{M}_Z^\dagger\right)$.

$$\overline{|\mathcal{M}_\gamma|^2} = 2e^4 \frac{s^2+u^2}{t^2}, \tag{2.43}$$

$$\overline{|\mathcal{M}_Z|^2} = \frac{e^4}{8c_W^4 s_W^4} \frac{1}{\left(t-m_Z^2\right)^2} \left[\left((g_V^e)^2+(a_V^e)^2\right)\left((g_V^\mu)^2+(a_V^\mu)^2\right)\left(s^2+u^2\right) + 4g_V^e g_V^\mu a_V^e a_V^\mu \left(s^2-u^2\right)\right] \tag{2.44}$$

$$\text{and} \quad \sum_{\text{spin}} \Re\left(\mathcal{M}_\gamma \mathcal{M}_Z^\dagger\right) = \frac{e^4}{2c_W^2 s_W^2} \frac{1}{t\left(t-m_Z^2\right)} \left(-2g_V^e g_V^\mu \left(s^2+u^2\right) - 2a_V^e a_V^\mu \left(s^2-u^2\right)\right). \tag{2.45}$$

All three amplitudes have terms dependent on s^2 and u^2. More specifically contributions linear in $\left(s^2+u^2\right)$ and $\left(s^2-u^2\right)$.

2.2. Electron-Quark Scattering

One way of examining electron-quark scattering, as seen in Fig. 3, in the first place is to transfer the solution of $e^-\mu^- \to e^-\mu^-$ scattering to $e^-q \to e^-q$. Quarks are spin-$\frac{1}{2}$, this means the wave function of the ingoing and outgoing particle stay $u(k_1)$ and $u(k_2)$. Also, the propagators do not change. The only difference is in the vertices. Before, all charges were $-1 \cdot e$. The fractional charge of quarks e_q is different and will be $+\frac{2}{3} \cdot e$ or $-\frac{1}{3} \cdot e$ depending on the type of quark. Also, for quarks we have to sum (and average) over color. The solution has no difference in color and so averaging cancels the sum. The quick solution is

$$\overline{|\mathcal{M}_\gamma|^2} = 2e^4 e_q^2 \frac{s^2+u^2}{t^2}, \tag{2.46}$$

$$\overline{|\mathcal{M}_Z|^2} = \frac{e^4 e_q^2}{8c_W^4 s_W^4} \frac{1}{\left(t-m_Z^2\right)^2} \left[\left((g_V^e)^2+(a_V^e)^2\right)\left((g_V^q)^2+(a_V^q)^2\right)\left(s^2+u^2\right) + 4g_V^e g_V^q a_V^e a_V^q \left(s^2-u^2\right)\right] \tag{2.47}$$

$$\text{and} \quad \sum_{\text{spin}} \Re\left(\mathcal{M}_\gamma \mathcal{M}_Z^\dagger\right) = \frac{e^4 e_q^2}{2c_W^2 s_W^2} \frac{1}{t\left(t-m_Z^2\right)} \left(-2g_V^e g_V^q \left(s^2+u^2\right) - 2a_V^e a_V^q \left(s^2-u^2\right)\right). \tag{2.48}$$

One remark before continuing: The change might not seem big, but it is easy to oversee the different coupling indices. g_V^q and a_V^q are different to g_V^μ and a_V^μ.

Now we want to broaden our horizon. Already we have calculated the amplitude for $e^- q \to e^- q$ scattering. But when dealing with an accelerator, it is not the only interaction that can happen. There might be a charged current propagating between the particles. The four interactions $e^-(u,c) \to \nu_e(d,s)$ and $e^-(d,s) \to \overline{\nu}_e(u,c)$ suddenly emerge. To conclude, we now want to cover $e^\pm p$ scattering for vector bosons, namely γ, Z and $W^\pm$, for neutral current and charged current. The diagrams are shown in Fig. 4 and all here considered interactions are listed in Table 1. Interactions with initial electron neutrino ν_e are not included here, because we won't compare to such data.

Table 1: All possible, considered interactions.

	$e^+;\ \gamma, Z$	$e^-;\ \gamma, Z$	$e^-;\ W^-$	$e^+;\ W^+$
u	$e^+u \overset{\gamma,Z}{\to} e^+u$	$e^-u \overset{\gamma,Z}{\to} e^-u$	$e^-u \overset{W^-}{\to} \nu_e d$	
c	$e^+c \overset{\gamma,Z}{\to} e^+c$	$e^-c \overset{\gamma,Z}{\to} e^-c$	$e^-c \overset{W^-}{\to} \nu_e s$	
d	$e^+d \overset{\gamma,Z}{\to} e^+d$	$e^-d \overset{\gamma,Z}{\to} e^-d$		$e^+d \overset{W^+}{\to} \overline{\nu}_e u$
s	$e^+s \overset{\gamma,Z}{\to} e^+s$	$e^-s \overset{\gamma,Z}{\to} e^-s$		$e^+s \overset{W^+}{\to} \overline{\nu}_e c$
$\overline{u}$	$e^+\overline{u} \overset{\gamma,Z}{\to} e^+\overline{u}$	$e^-\overline{u} \overset{\gamma,Z}{\to} e^-\overline{u}$		$e^+\overline{u} \overset{W^+}{\to} \overline{\nu}_e \overline{d}$
$\overline{c}$	$e^+\overline{c} \overset{\gamma,Z}{\to} e^+\overline{c}$	$e^-\overline{c} \overset{\gamma,Z}{\to} e^-\overline{c}$		$e^+\overline{c} \overset{W^+}{\to} \overline{\nu}_e \overline{s}$
$\overline{d}$	$e^+\overline{d} \overset{\gamma,Z}{\to} e^+\overline{d}$	$e^-\overline{d} \overset{\gamma,Z}{\to} e^-\overline{d}$	$e^-d \overset{W^-}{\to} \nu_e \overline{u}$	
$\overline{s}$	$e^+\overline{s} \overset{\gamma,Z}{\to} e^+\overline{s}$	$e^-\overline{s} \overset{\gamma,Z}{\to} e^-\overline{s}$	$e^-\overline{s} \overset{W^-}{\to} \nu_e \overline{c}$	

2.2.1. Generalized Leptonic Tensor

We can calculate all amplitudes from Table 1 in a generalized fashion. This way the invariant amplitudes can quickly be solved and calculations won't be so long as up to here. A generalized leptonic tensor shall be determined in this section. It will have a structure able to cover parity-violating terms yielded by the bosons. This was inspired by Eq. 15.112 in [Kov]. To cover separate contributions in parity, the general leptonic tensor has the form

$$\tilde{L}^{\mu\nu}(p_A, p_B) = \frac{1}{2} \sum_{\text{spins}} \left(\overline{u}(p_B)\left(A_L \gamma^\mu P_L + A_R \gamma^\mu P_R\right) u(p_A)\right) \left(\overline{u}(p_B)\left(B_L \gamma^\nu P_L + B_R \gamma^\nu P_R\right) u(p_A)\right)^*. \tag{2.49}$$

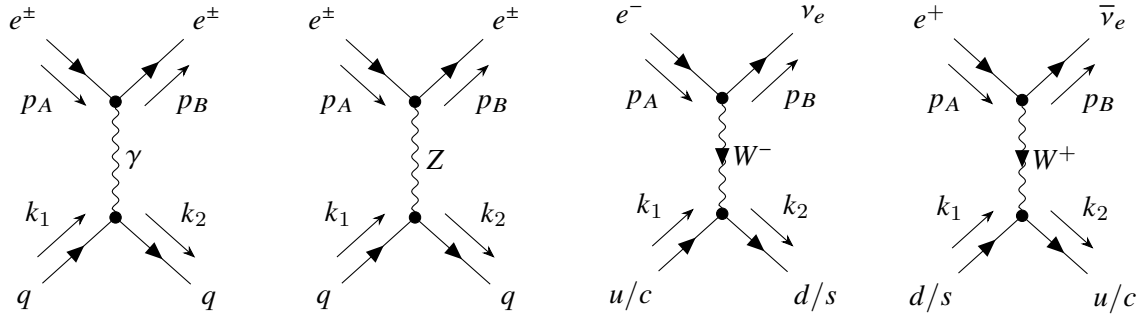

(a) Electromagnetic, neutral current.

(b) Electroweak, neutral current.

(c) Electroweak, charged current.

(d) Electroweak, charged current.

Figure 4: $e^\pm q$ scattering in lowest order. Neutral current $e^\pm q$ scatt. is composed out of he left half diagrams (Figs. 4a and 4b) and charged current e^- displayed in Fig. 4c, e^+ in Fig. 4d.

$A_{L/R}$ and $B_{L/R}$ are the parts that depict the diverse behavior under helicity. Repeat the procedure from Section 2.1. For the conjugation we use the following rules: $\left\{\gamma^5, \gamma^\xi\right\} = 0 \Rightarrow \left\{P_{L/R}, \gamma^\xi\right\} = 0$

$$\left(\overline{u}(p_B)\left(B_L\gamma^\nu P_L + B_R\gamma^\nu P_R\right)u(p_A)\right)^* = u^\dagger(p_A)\left(B_L P_L \gamma^{\nu\dagger} + B_R P_R \gamma^{\nu\dagger}\right)\gamma^0\overline{u}^\dagger(p_B) \tag{2.50}$$

$$= \overline{u}(p_A)\gamma^0\left(B_L P_R \gamma^\nu + B_R P_L \gamma^\nu\right)u(p_B) \tag{2.51}$$

$$= \overline{u}(p_A)\left(B_L\gamma^\nu P_L + B_R\gamma^\nu P_R\right)u(p_B) \tag{2.52}$$

To evaluate we make use of trace theorems from Appendix A.2 and Appendix A.1 namely $\sum_{\text{spin}} u(k)\overline{u}(k) = \not{k} + m$ and $\sum_{\text{spin}} v(k)\overline{v}(k) = \not{k} - m$, while neglecting the masses they are the same. This means there is no difference for particles and antiparticles.

$$\tilde{L}^{\mu\nu} = \frac{1}{2}\sum_{\text{spins}}\left(\overline{u}(p_B)\left(A_L\gamma^\mu P_L + A_R\gamma^\mu P_R\right)u(p_A)\right)\left(\overline{u}(p_A)\left(B_L\gamma^\nu P_L + B_R\gamma^\nu P_R\right)u(p_B)\right) \tag{2.53}$$

$$= \frac{1}{2}\sum_{\text{spins}}\left[u(p_B)\overline{u}(p_B)\right]\left(A_L\gamma^\mu P_L + A_R\gamma^\mu P_R\right)\left[u(p_A)\overline{u}(p_A)\right]\left(B_L\gamma^\nu P_L + B_R\gamma^\nu P_R\right) \tag{2.54}$$

$$= \frac{1}{2}\operatorname{Tr}\{\not{p}_B\left(A_L\gamma^\mu P_L + A_R\gamma^\mu P_R\right)\not{p}_A\left(B_L\gamma^\nu P_L + B_R\gamma^\nu P_R\right)\} \tag{2.55}$$

P_L and P_R are projection operators for chirality as shown in Appendix A.3, so:

$$= \frac{1}{2}\left(A_L B_L \operatorname{Tr}\{\not{p}_B\gamma^\mu\not{p}_A\gamma^\nu P_L\} + A_R B_R \operatorname{Tr}\{\not{p}_B\gamma^\mu\not{p}_A\gamma^\nu P_R\}\right) \tag{2.56}$$

$$= \frac{1}{4}\left(\left(A_L B_L + A_R B_R\right)\operatorname{Tr}\{\not{p}_B\gamma^\mu\not{p}_A\gamma^\nu\} + \left(-A_L B_L + A_R B_R\right)\operatorname{Tr}\left\{\not{p}_B\gamma^\mu\not{p}_A\gamma^\nu\gamma^5\right\}\right) \tag{2.57}$$

$$= \left(A_L B_L + A_R B_R\right)\left(p_A^\mu p_B^\nu + p_B^\mu p_A^\nu - (p_A p_B)\, g^{\mu\nu}\right) + i\left(A_L B_L - A_R B_R\right)p_{A,\rho}p_{B,\sigma}\epsilon^{\mu\nu\rho\sigma} \tag{2.58}$$

For the photon exchange the general couplings are $A_{L/R} = B_{L/R} = e$ so

$$\tilde{L}^{\mu\nu}_{\gamma\gamma} = 2e^2\left(p_A^\mu p_B^\nu + p_B^\mu p_A^\nu - (p_A p_B)\, g^{\mu\nu}\right), \tag{2.59}$$

the interference term with $A_{L/R} = e$ and $B_{L/R} = \frac{g}{2c_W}(g_V \pm a_V)$ evaluates to

$$\tilde{L}^{\mu\nu}_{\gamma Z} = \tilde{L}^{\mu\nu}_{Z\gamma} = \frac{eg}{2c_W}\left(2g_V\left(p_A^\mu p_B^\nu + p_B^\mu p_A^\nu - (p_A p_B)\, g^{\mu\nu}\right) + 2ia_V p_{A,\rho} p_{B,\sigma}\epsilon^{\mu\nu\rho\sigma}\right). \tag{2.60}$$

Knowing $g = \frac{e}{s_W}$ this equals

$$= \frac{e^2}{c_W s_W}\left(g_V\left(p_A^\mu p_B^\nu + p_B^\mu p_A^\nu - (p_A p_B)\, g^{\mu\nu}\right) + ia_V p_{A,\rho} p_{B,\sigma}\epsilon^{\mu\nu\rho\sigma}\right). \tag{2.61}$$

For the Z exchange both $A_{L/R} = B_{L/R} = \frac{g}{2c_W}(g_V \pm a_V)$

$$\tilde{L}^{\mu\nu}_{ZZ} = \frac{e^2}{4c_W^2 s_W^2}\left[2\left(g_V^2 + a_V^2\right)\left(p_A^\mu p_B^\nu + p_B^\mu p_A^\nu - (p_A p_B)\, g^{\mu\nu}\right) + 4ig_V a_V p_{A,\rho} p_{B,\sigma}\epsilon^{\mu\nu\rho\sigma}\right]. \tag{2.62}$$

Lastly for the $W^\pm$ exchange $A_L = B_L = \frac{g}{\sqrt{2}}$ and $A_R = B_R = 0$, where $g = \frac{e}{s_W}$, thus (see vertex factor in Appendix A.4)

$$\tilde{L}^{\mu\nu}_{W} = \frac{g^2}{2}\left(p_A^\mu p_B^\nu + p_B^\mu p_A^\nu - (p_A p_B) g^{\mu\nu} + ip_{A,\rho} p_{B,\sigma}\epsilon^{\mu\nu\rho\sigma}\right). \tag{2.63}$$

This already shows the benefit of the general leptonic tensor. To get to the invariant amplitude is only one step away.

2.2.2. Invariant Amplitudes

The goal is to acquire four different invariant amplitudes: $e^\pm q$ with neutral current $\overline{|\mathcal{M}^\pm_{\mathrm{NC}}|^2} = \overline{|\mathcal{M}^\pm_\gamma|^2} + \sum_{\mathrm{spin}} \Re\left(\mathcal{M}^\pm_\gamma \mathcal{M}^{\pm\dagger}_Z\right) + \overline{|\mathcal{M}^\pm_Z|^2}$ and $e^\pm q$ with charged current $\overline{|\mathcal{M}^\pm_{\mathrm{CC}}|^2} = \overline{|\mathcal{M}^\pm_W|^2}$.
As a refresher: the definitions for the coupling coefficients and axial/vector couplings stay the same. e_f is the particle charge in units $|e|$,

$$C_L = I_f^{3L} - e_f \sin\theta_W \qquad \text{and} \qquad C_R = -e_f \sin\theta_W \tag{2.64}$$

where I_f^{3L} is the weak isospin of the fermion. The second parameterization is:

$$g_v = C_L + C_R = I_f^{3L} - 2e_f \sin\theta_W, \qquad a_v = C_L - C_R = I_f^{3L}. \tag{2.65}$$

For simplicity, we take the constants for the electron e^-. This way the sign in the amplitudes index smoothly transfers to the actual outcome, without changing constants.
With the Feynman rules, the diagrams in Fig. 4 can be evaluated to

$$\mathcal{M}^\pm_\gamma = \overline{u}(p_B)(ie)\gamma^\mu u(p_A) \cdot \frac{g_{\mu\nu}}{(p_A - p_B)^2} \cdot \overline{u}(k_2)(iee_q)\gamma^\nu u(k_1) \tag{2.66}$$

$$\overline{|\mathcal{M}^\pm_\gamma|^2} = \frac{e_q^2}{t^2}\tilde{L}^{\mu\nu}_{\gamma\gamma}(p_A, p_B)\tilde{L}^{\mu\nu}_{\gamma\gamma}(k_1, k_2) g_{\mu\nu} \tag{2.67}$$

$$= \frac{4e^4e_q^2}{t^2}\left(p_A^\mu p_B^\nu + p_B^\mu p_A^\nu - (p_Ap_B)\,g^{\mu\nu}\right)\left(k_{1,\mu}k_{2,\nu} + k_{2,\mu}k_{1,\nu} - (k_1k_2)\,g_{\mu\nu}\right) \tag{2.68}$$

$$= \frac{4e^4e_q^2}{t^2}\big(2\,(p_Ak_1)\,(p_Bk_2) + 2\,(p_Ak_2)\,(p_Bk_1) - 2\,(p_Ap_B)\,(k_1k_2) - 2\,(k_1k_2)\,(p_Ap_B) + 4\,(p_Ap_B)\,(k_1k_2)\big) \tag{2.69}$$

$s = (p_A + k_1)^2 \simeq 2p_Ak_1$, $u = (p_A + k_2)^2 \simeq 2p_Ak_2$

$$= \frac{4e^4e_q^2}{t^2}2\big(\underbrace{(p_Bk_2)}_{\frac{s}{2}}\underbrace{(p_Ak_1)}_{\frac{s}{2}} + \underbrace{(p_Bk_1)}_{-\frac{u}{2}}\underbrace{(p_Ak_2)}_{-\frac{u}{2}}\big) \;= 2e^4e_q^2\frac{s^2+u^2}{t^2}. \tag{2.70}$$

The solution is equal to one of the first calculation in Section 2.1.1. For the Z boson

$$\mathcal{M}_Z^\pm = \overline{u}(p_B)\left(\frac{ig}{\cos\theta_W}\right)\gamma^\mu\left(C_L^{e^\pm}P_L + C_R^{e^\pm}P_R\right)u(p_A)\cdot\frac{g_{\mu\nu}}{t-m_Z^2}\cdot\overline{u}(k_2)\left(\frac{ig}{\cos\theta_W}\right)\gamma^\nu\left(C_L^qP_L + C_R^qP_R\right)u(k_1). \tag{2.71}$$

For particles the second leptonic tensor is $\tilde{L}_{ZZ}^{\mu\nu}(k_1,k_2)$, for antiparticles k_1 and k_2 swap. This causes two possible signs further on. The upper one describes particles, the lower one antiparticles.

$$\overline{|\mathcal{M}_Z^\pm|^2} = \frac{1}{\left(t-m_Z^2\right)^2}\tilde{L}_{ZZ}^{\mu\nu}\tilde{L}_{ZZ}^{\mu\nu}g_{\mu\nu} \tag{2.72}$$

$$= \frac{e^4}{\left(t-m_Z^2\right)^2}\frac{1}{16c_W^4s_W^4}\Big[4\left(g_V^{e^-\,2} + a_V^{e^-\,2}\right)\left(g_V^{q\,2} + a_V^{q\,2}\right)\left(2\,(p_Ak_1)\,(p_Bk_2) + 2\,(p_Ak_2)\,(p_Bk_1)\right) \pm 16g_V^{e^-}g_V^qa_V^{e^-}a_V^qp_{A,\rho}p_{B,\sigma}k_{1,\alpha}k_{2,\beta}\epsilon^{\mu\nu\rho\sigma}\epsilon_{\mu\nu\alpha\beta}\Big] \tag{2.73}$$

$$p_{A,\rho}p_{B,\sigma}k_{1,\alpha}k_{2,\beta}\epsilon^{\mu\nu\rho\sigma}\epsilon_{\mu\nu\alpha\beta} = -p_{A,\rho}p_{B,\sigma}k_{1,\alpha}k_{2,\beta}2\left(\delta_\alpha^\rho\delta_\beta^\sigma - \delta_\beta^\rho\delta_\alpha^\sigma\right) = -2\left((p_Bk_2)\,(p_Ak_1) - (p_Bk_1)\,(p_Ak_2)\right)$$

$$= \frac{e^4}{\left(t-m_Z^2\right)^2}\frac{1}{16c_W^4s_W^4}\left[2\left(g_V^{e^-\,2} + a_V^{e^-\,2}\right)\left(g_V^{q\,2} + a_V^{q\,2}\right)\left(s^2+u^2\right) \mp 8g_V^{e^-}g_V^qa_V^{e^-}a_V^q\left(s^2-u^2\right)\right]. \tag{2.74}$$

Equaling the first calculated amplitude. The interference term evaluates much quicker now, too:

$$\sum_{\text{spin}}\Re\left(\mathcal{M}_\gamma^\pm\mathcal{M}_Z^{\pm\dagger}\right) = \frac{2e_q}{t\left(t-m_Z^2\right)}\tilde{L}_{\gamma Z}^{\mu\nu}(p_A,p_B)\tilde{L}_{\gamma Z}^{\mu\nu}(k_1,k_2)g_{\mu\nu} \tag{2.75}$$

$$= \frac{2e^4e_q}{t\left(t-m_Z^2\right)}\frac{1}{4c_W^2s_W^2}\big(-2g_V^{e^-}g_V^q\left((p_Ak_1)\,(p_Bk_2) + (p_Ak_2)\,(p_Bk_1)\right) \mp 2a_V^{e^-}a_V^q\left((p_Ak_2)\,(p_Bk_1) - (p_Ak_1)\,(p_Bk_2)\right)\big) \tag{2.76}$$

$$= \frac{2e^4e_q}{t\left(t-m_Z^2\right)}\frac{1}{4c_W^2s_W^2}\left(-2g_V^{e^-}g_V^q\left(s^2+u^2\right) \pm 2a_V^{e^-}a_V^q\left(s^2-u^2\right)\right) \tag{2.77}$$

m_W is the W boson mass. For the charged current a difference in quark/antiquark scattering emerges. When assembling $\mathcal{M}$ for antiparticles, the order of multiplication is inverse to the same for particles. The Levi-Civita-Tensor in $\tilde{L}_W^{\mu\nu}$ isn't interchangeable without a change in signs. There are four different configurations: $(p_A, p_B)(k_1, k_2)$, $(p_A, p_B)(k_2, k_1)$, $(p_B, p_A)(k_1, k_2)$ and $(p_B, p_A)(k_2, k_1)$. The result is

$$\overline{|\mathcal{M}_W^{\pm}|^2} = \frac{1}{\left(t - m_W^2\right)^2} \tilde{L}_W^{\mu\nu} \tilde{L}_W^{\mu\nu} g_{\mu\nu} \tag{2.78}$$

$$= \frac{e^4}{\left(t - m_W^2\right)^2} \frac{1}{s_W^4} \left(2\left(p_A k_1\right)\left(p_B k_2\right) + 2\left(p_A k_2\right)\left(p_B k_1\right) \mp p_{A,\rho} p_{B,\sigma} k_{1,\alpha} k_{2,\beta} \epsilon^{\mu\nu\rho\sigma} \epsilon_{\mu\nu\alpha\beta}\right) \tag{2.79}$$

$$= \frac{e^4}{\left(t - m_W^2\right)^2} \frac{1}{s_W^4} \left(\frac{s^2 + u^2}{2} \mp \frac{s^2 - u^2}{2}\right) \tag{2.80}$$

The sign in $\overline{|\mathcal{M}_W^{\pm}|^2}$ describes the $e^{\pm}$, but the sign in the resulting expression is $+$ for particle-particle, antiparticle-antiparticle and $-$ for the other two scatterings.

3. Electron-Proton Scattering

After all these preliminaries, we can finally stitch the pieces together. The electron-proton scattering is viewed at large energy transfers $Q^2 = -q^2 \gg M^2$ ("Deep") and for the proton breaking up, that is at a large invariant mass of the collision debris $W^2 \gg M^2$ ("Inelastic"). In Fig. 5 we draw a diagram to show the corresponding relevant variables. According to the parton model, the proton cross section can be written as a sum of incoherent quark scattering like [HM84, p. 193, 9.17]

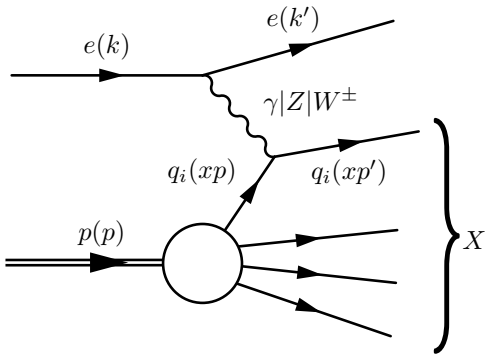

Figure 5: Inelastic electron-proton scattering.[4]

$$\left(\frac{\mathrm{d}\sigma^{e^\pm p}}{\mathrm{d}x\,\mathrm{d}Q^2}\right)_{ep\to eX} = \sum_q \int_0^1 \mathrm{d}\xi f_q(\xi) \left(\frac{\mathrm{d}\hat{\sigma}^q}{\mathrm{d}x\,\mathrm{d}Q^2}\right)_{eq_i\to eq_i} \tag{3.1}$$

with the probability $f_q(\xi)$ of finding quark q with the momentum fraction ξ.
The inelastic scattering neglecting the mass of the proton compared to the energy of the incoming lepton can be written in this general form [Kov, p. 227, 15.127]

$$\begin{aligned}\frac{\mathrm{d}\sigma}{\mathrm{d}x\,\mathrm{d}Q^2} &= \frac{2\pi\alpha^2}{xQ^4}\left[(2xF_1 - F_2)\,y^2 + \left(1 + (1-y)^2\right) F_2 \pm \left(1 - (1-y)^2\right) xF_3\right] \\ &= \frac{2\pi\alpha^2}{xQ^4}\left[Y_+ F_2 - y^2 F_L \pm Y_- xF_3\right]\end{aligned} \tag{3.2}$$

where $Y_\pm = 1 \pm (1-y)^2$ and $F_L = F_2 - 2xF_1$. $F_1(x,Q^2)$, $F_2(x,Q^2)$, and $F_3(x,Q^2)$ are called form factors and are in general functions of the momentum fraction x and the energy transfer Q^2. Dependent on the interaction they contribute differently.
One can simplify the elastic partonic cross section using invariant kinematic variables. The transformation is

$$\frac{\mathrm{d}\hat{\sigma}^{e^\pm q}}{\mathrm{d}x\,\mathrm{d}Q^2} = -\frac{1}{Q^2}\frac{\mathrm{d}\hat{\sigma}^{e^\pm q}}{\mathrm{d}\hat{t}}\delta(x-\xi)\,. \tag{3.3}$$

where the δ-function sets ξ to the Bjorken x, see [Mar94, p. 9]. For the following fractional Mandelstam variables with hats are introduced

$$\hat{s} = (xp+k)^2 \simeq 2xpk \simeq xs, \quad \hat{t} = -Q^2 = -xys, \quad \hat{u} = -\hat{s} - \hat{u} = -x(1-y)\,s \tag{3.4}$$

where $y = \frac{2pq}{s} = \frac{Q^2}{xs}$. Now the invariant amplitudes from Section 2.2.2 will be incorporated to a differential cross section so that it is possible to compare them with measured data.

[4] This one diagram was drawn using `feynmp` [Ohl96].

3.1. Neutral Current

$$\begin{aligned}\frac{\mathrm{d}^2\hat{\sigma}^{e^\pm q}_{\mathrm{NC}}}{\mathrm{d}\hat{t}} &= \frac{1}{16\pi\hat{s}^2}\left(\overline{|\mathcal{M}^\pm_\gamma|^2} + \overline{|\mathcal{M}^\pm_{\gamma Z}|^2} + \overline{|\mathcal{M}^\pm_Z|^2}\right) = \frac{1}{16\pi\hat{s}^2}\overline{|\mathcal{M}^\pm_{\mathrm{NC}}|^2} \\ &= \frac{1}{16\pi\hat{s}^2}\Bigg(2e^4e_q^2\frac{\hat{s}^2+\hat{u}^2}{\hat{t}^2} + \frac{2}{\hat{t}\left(\hat{t}-m_Z^2\right)}\frac{e^4e_q}{4c_W^2s_W^2}\left(-2g_V^{e^-}g_V^q\left(\hat{s}^2+\hat{u}^2\right) \pm 2a_V^{e^-}a_V^q\left(\hat{s}^2-\hat{u}^2\right)\right) \\ &\quad + \frac{1}{\left(\hat{t}-m_Z^2\right)^2}\frac{e^4}{16c_W^4s_W^4}\left(2\left(g_V^{e^-\,2}+a_V^{e^-\,2}\right)\left(g_V^{q\,2}+a_V^{q\,2}\right)\left(\hat{s}^2+\hat{u}^2\right) \mp 8g_V^{e^-}g_V^qa_V^{e^-}a_V^q\left(\hat{s}^2-\hat{u}^2\right)\right)\Bigg),\end{aligned} \tag{3.5}$$

With $\frac{\hat{s}^2\pm\hat{u}^2}{\hat{s}^2} = 1 \pm \frac{x^2(1-y)^2s^2}{x^2s^2} = 1 \pm (1-y)^2$ the differential cross section is transferred in an equivalent base using only y. For a measurement, it is rather easy to determine y.

$$\begin{aligned}\frac{\mathrm{d}^2\hat{\sigma}^{e^\pm q}_{\mathrm{NC}}}{\mathrm{d}x\,\mathrm{d}Q^2} &= \frac{2\pi\alpha^2}{Q^4}\Bigg(e_q^2\left\{1+(1-y)^2\right\} + \frac{e_q}{c_W^2s_W^2}\frac{\hat{t}}{\hat{t}-m_Z^2}\left(\pm 2g_V^{e^-}g_V^q\left\{1+(1-y)^2\right\} - 2a_V^{e^-}a_V^q\left\{1-(1-y)^2\right\}\right) \\ &+ \frac{1}{32c_W^4s_W^4}\frac{\hat{t}^2}{\left(\hat{t}-m_Z^2\right)^2}\left(2\left(g_V^{e^-\,2}+a_V^{e^-\,2}\right)\left(g_V^{q\,2}+a_V^{q\,2}\right)\left\{1+(1-y)^2\right\} \mp 8g_V^{e^-}g_V^qa_V^{e^-}a_V^q\left\{1-(1-y)^2\right\}\right)\Bigg) \\ &\cdot\,\delta\left(x-\xi\right).\end{aligned} \tag{3.6}$$

Table 2: The fractional charge of the electron and U-, D-type quarks. For the antiparticles the sign of both the electrical charge and weak isospin changes.

	e^-	U	D
e_f	-1	$+\frac{2}{3}$	$-\frac{1}{3}$
I_f^{3L}, a_V^f	$-\frac{1}{2}$	$+\frac{1}{2}$	$-\frac{1}{2}$
g_V^f	$-\frac{1}{2}+2s_W$	$+\frac{1}{2}-\frac{4}{3}s_W$	$-\frac{1}{2}+\frac{2}{3}s_W$

3.2. Charged Current

For the charged current, the quark sum acts differently. Charged current here describes the interactions in the two most right columns in Table 1. Depending on whether or not the ingoing two particles are antiparticles. The distinction between U- and D-type quarks as shown in Table 2 generalizes the quark situation appropriately. Again only quarks below the b-quark mass threshold are minded. Particles of greater mass shouldn't play a significant role in the processes. xU is the sum of up- and charm-quark distributions and xD the sum of down- and strange-quarks. The antiparticles are of course the sum of the anti-quarks.

$$xU = xu + xc \qquad x\overline{U} = x\overline{u} + x\overline{c} \qquad xD = xd + xs \qquad x\overline{D} = x\overline{d} + x\overline{s} \tag{3.7}$$

For the differential cross sections then the following holds:

$$\begin{aligned}\frac{\mathrm{d}^2\sigma_{\mathrm{CC}}^{e^+p}}{\mathrm{d}x\,\mathrm{d}Q^2} &= \frac{1}{16\pi\hat{s}^2}\left(\overline{|\mathcal{M}_W^{\overline{U}}|^2} f_{\overline{U}}(x) + \overline{|\mathcal{M}_W^{D}|^2} f_D(x)\right) \\ &= \frac{1}{16\pi}\frac{1}{\left(\hat{t}+m_W^2\right)^2}\frac{e^4}{s_W^4}\left(\frac{\hat{s}^2}{\hat{s}^2} f_{\overline{U}}(x) + \frac{\hat{u}^2}{\hat{s}^2} f_D(x)\right) \qquad (3.8)\\ \frac{\mathrm{d}^2\sigma_{\mathrm{CC}}^{e^-p}}{\mathrm{d}x\,\mathrm{d}Q^2} &= \frac{1}{16\pi}\frac{1}{\left(\hat{t}+m_W^2\right)^2}\frac{e^4}{s_W^4}\left(\frac{\hat{s}^2}{\hat{s}^2} f_U(x) + \frac{\hat{u}^2}{\hat{s}^2} f_{\overline{D}}(x)\right) \qquad (3.9)\end{aligned}$$

To move into the common base $\frac{\hat{u}^2}{\hat{s}^2} = \frac{x^2(1-y)^2s^2}{x^2s^2} = (1-y)^2$ does the trick.

4. PDF Comparisons

And finally, we will compare the results with measured data. The latest data on DIS come from the H1 and ZEUS Collaborations which have performed $e^{\pm}p$ scattering experiments with nearly 4π coverage and published data for the charged and neutral current including interference effects [HZ15]. The tactic is the following. We will use our calculation coupled to different PDFs and compare the predicitions to HERA data.
The compared sets are CTEQ6 from 2002 [Pum+02], CT10 from 2010 [Lai+10] and CT18NNLO from 2019 [Hou+19]. The three come from the Coordinated Theoretical-Experimental Project on QCD (CTEQ). Also HERAPDF20_LO_EIG (2015) from the H1 and ZEUS Collaborations will be examined, as the group responsible for the data against which we compare.
First the data from HERA [HZ15] are given in the form of the reduced neutral-current cross section

$$\sigma^{\pm}_{r,\mathrm{NC}} = \frac{\mathrm{d}^2\sigma^{e^{\pm}p}_{\mathrm{NC}}}{\mathrm{d}x\,\mathrm{d}Q^2}\cdot\frac{Q^4 x}{2\pi\alpha^2 Y_+} = -\frac{y^2}{Y_+}\tilde{F}_L + \tilde{F}_2 \mp \frac{Y_-}{Y_+}x\tilde{F}_3, \tag{4.1}$$

where $Y_{\pm}$ are shorthands for $1 \pm (1-y)^2$. This form is equivalent to the one derived in Eq. (3.6). At leading order in this case $\tilde{F_L} = \tilde{F_2} - 2x\tilde{F_1} = 0$. For a more comprehensive notation, the paper suggests using

$$\begin{aligned} \tilde{F_2} &= F_2 - \kappa_Z g_V^{e^-}\cdot F_2^{\gamma Z} + \kappa_Z^2\left(g_V^{e^-\,2} + a_V^{e^-\,2}\right)\cdot F_2^Z \\ x\tilde{F_3} &= -\kappa_Z a_V^{e^-}\cdot xF_3^{\gamma Z} + \kappa_Z^2 2 g_V^{e^-} a_V^{e^-}\cdot xF_3^Z. \end{aligned} \tag{4.2}$$

After a comparison of our form factors to their notation

$$\begin{aligned} F_2 &= \sum_q e_q^2 f_q(x), & F_2^{\gamma Z} &= 2\sum_q e_q g_V^q f_q(x), & F_2^Z &= \sum_q \left(g_V^{q\,2} + a_V^{q\,2}\right) f_q(x), \\ & & xF_3^{\gamma Z} &= 2\sum_q e_q a_V^q f_q(x), & xF_3^Z &= 2\sum_q g_V^q a_V^q f_q(x). \end{aligned} \tag{4.3}$$

The H1 and ZEUS Collaborations also published data for the charged current in a reduced form

$$\sigma^{\pm}_{r,\mathrm{CC}} = \frac{2\pi x}{G_F^2}\left[\frac{m_W^2 + Q^2}{m_W^2}\right]^2 \frac{\mathrm{d}^2\sigma^{e^{\pm}p}_{\mathrm{CC}}}{\mathrm{d}x\,\mathrm{d}Q^2}, \tag{4.4}$$

with the Fermi coupling constant $G_F = \frac{\pi\alpha}{\sqrt{2}s_W^2 m_W^2}$. For us that means

$$\sigma^{+}_{r,\mathrm{CC}} = 4\pi\left(x f_{\overline{U}}(x) + (1-y)^2 x f_D(x)\right), \tag{4.5}$$

$$\sigma^{-}_{r,\mathrm{CC}} = 4\pi\left(x f_U(x) + (1-y)^2 x f_{\overline{D}}(x)\right). \tag{4.6}$$

4.1. Numerics

Before we can compare anything we have to calculate the cross sections numerically. This is done with function definitions in python3. The code starts with imports. Later on, we should calculate the cross sections with uncertainties. For this, the type `ufloat`, a float with uncertainty, is imported. Two functions from `numpy` will be needed.

```
# Imports
from uncertainties import ufloat as uf
from numpy import arange, sqrt
```

Secondly, we define necessary natural constants. And s_W, c_W^2, c_W are deduced from s_W^2. We neglect the uncertainties of m_Z and s_W^2, because they are in a small enough magnitude. We take both from the last "Review of Particle Physics" [PDG+20b]. We then copy axial and vector couplings from Table 2.

```
# Natural Constants
mZ  = 91.1876  # ,0.0021)   # GeV - Z-Boson mass                 mZ
sW2 = 0.23121  # ,0.00004)  # 1   - sin(weak-mixing angle)^2     sW^2
sW  = sW2 ** (1 / 2)        # 1   - sin(weak-mixing angle)       sW
cW2 = 1 - sW2               # 1   - cos(weak-mixing angle)^2     cW^2
cW  = cW2 ** (1 / 2)        # 1   - cos(weak-mixing angle)       cW
# Axial and Vector Couplings
v_e = -1 / 2 + 2 * sW  # Electron   g_V^e
a_e = -1 / 2                      # a_V^e
e_u = +2 / 3  # Up-type             e_u
v_u = +1 / 2 - 4 / 3 * sW         # g_V^u
a_u = +1 / 2                      # a_V^u
e_d = -1 / 3  # Down-type           e_d
v_d = -1 / 2 + 2 / 3 * sW         # g_V^d
a_d = -1 / 2                      # a_V^d
```

Before continuing to the cross sections, we define auxiliary functions. The functions are k_Z, y and $Y_\pm$ from the prior notation.

```
# Auxiliary functions
def k_Z(Q2): return (4 * cW2 * sW2) ** (-1) * (Q2) / (Q2 + mZ ** 2)  # 1   - Q in GeV
def y(Q2, x, s): return Q2 / (x * s)  # 1   - Q in GeV, x-Bjorken, s in GeV^2
def Y(sign, Q2, x, s): return 1 + sign * (1 - y(Q2, x, s)) ** 2
                      # 1 - sign of Y±, Q in GeV, x-Bjorken, s in GeV^2
```

First, we implement a version of the cross sections without the uncertainty, the reason for that is the way we calculate uncertainties with the PDFs on hand. To get a hold of PDFs and a consistent interface, we use the python implementation of LHAPDF6 [Buc+15]. Let's start with $\sigma^\pm_{\mathrm{NC}}$. When given a PDF of class `PDF()` the function will calculate the nominal/center value of $\sigma^\pm_{\mathrm{NC}}(Q^2, x, s)$

for that one point. The function only consists out of a return statement as Eq. (4.1).

```
57 def sigmaNC(sign, pdf, Q2, x, s):
58     """
59     :param sign:(-/+1)  Charge of incoming electron / positron
60     :param pdf: PDF()   General interface for access to parton density information
61     :param Q2:  float   Negative four-momentum-transfer squared in GeV^2
62     :param x:   float   Bjorken x
63     :param s:   float   Total center-of-mass energy in GeV^2
64     :return:    float   Neutral current cross section for given lhapdf.PDF
65     """
66     return F2(pdf, Q2, x) - sign * Y(-1, Q2, x, s) / Y(+1, Q2, x, s) * xF3(pdf, Q2, x)
```

The helper functions `F2` and `xF3` are also in the same form as analytically computed in Eq. (4.2). The PDF is handed down and $xf_q(x)$ here evaluated through `pdf.xfxQ2(pid, x, Q2)`. `pid` sets the quark kind after the Monte Carlo particle numbering scheme [PDG+20a]. They have been defined before as follows.

```
27 def F2(pdf, Q2, x):
28     """
29     :param pdf: PDF()   General interface for access to parton density information
30     :param Q2:  float   Negative four-momentum-transfer squared
31     :param x:   float   Bjorken x
32     :return:    float   Form Factor F_2 for
33     """
34     return ((e_u ** 2
35              - k_Z(Q2) * v_e * 2 * e_u * v_u
36              + k_Z(Q2) ** 2 * (v_e ** 2 + a_e ** 2) * (v_u ** 2 + a_u ** 2)
37              ) * (pdf.xfxQ2(2, x, Q2) + pdf.xfxQ2(4, x, Q2)      #        up, charm
38                   + pdf.xfxQ2(-2, x, Q2) + pdf.xfxQ2(-4, x, Q2)) # anti - up, charm
39             + (e_d ** 2
40                - k_Z(Q2) * v_e * 2 * e_d * v_d
41                + k_Z(Q2) ** 2 * (v_e ** 2 + a_e ** 2) * (v_d ** 2 + a_d ** 2)
42                ) * (pdf.xfxQ2(1, x, Q2) + pdf.xfxQ2(3, x, Q2)     #     down, strange
43                     + pdf.xfxQ2(-1, x, Q2) + pdf.xfxQ2(-3, x, Q2))#anti-down, strange
44             )
45
46 def xF3(pdf, Q2, x): # doc same to F2, but for xF3
47     return 2 * ((- k_Z(Q2) * a_e * e_u * a_u
48                  + k_Z(Q2) ** 2 * 2 * v_e * a_e * v_u * a_u
49                  ) * (pdf.xfxQ2(2, x, Q2) + pdf.xfxQ2(4, x, Q2)     #       up, charm
50                       - pdf.xfxQ2(-2, x, Q2) - pdf.xfxQ2(-4, x, Q2))# anti- up, charm
51                 + (- k_Z(Q2) * a_e * e_d * a_d
52                    + k_Z(Q2) ** 2 * 2 * v_e * a_e * v_d * a_d
53                    ) * (pdf.xfxQ2(1, x, Q2) + pdf.xfxQ2(3, x, Q2)     # down, strange
54                         - pdf.xfxQ2(-1, x, Q2) - pdf.xfxQ2(-3, x, Q2))
55                 )                                                  # anti - down, strange
```

For the charged current $\sigma^{\pm}_{\mathrm{CC}}$ the function is shorter. For σ^{+}_{CC} the variable `sign` has to be `+1`, for σ^{-}_{CC} it must be set to `-1`. The code then either realizes σ^{+}_{CC} (Eq. (4.5)) or σ^{-}_{CC} (Eq. (4.6)).

```
68 def sigmaCC(sign, pdf, Q2, x, s): # doc same as sigmaNC() but for charged current
69     return (
70             (pdf.xfxQ2(-sign * 2, x, Q2) + pdf.xfxQ2(-sign * 4, x, Q2)) # up, charm
71             + (1 - y(Q2, x, s)) ** 2 *
72             (pdf.xfxQ2(sign * 1, x, Q2) + pdf.xfxQ2(sign * 3, x, Q2)) # down, strange
73     )
```

Now for the functions with uncertainty, a list of different PDFs is given. The nominal value is calculated using the zeroth PDF in the list, the best fit S_0. The uncertainty can be calculated from the formula

$$\Delta\sigma = \frac{1}{2}\left(\sum_{i=1}^{N_P}\left[\sigma\left(S_i^+\right) - \sigma\left(S_i^-\right)\right]^2\right)^{1/2} \tag{4.7}$$

where $S_i^{\pm}$ are the error PDFs. When creating a PDF there are different parameters. The other PDFs $S_i^{\pm}$ consist out of functions where the fit parameters are offset by their uncertainty. Once in the positive direction S_i^+ and once in the negative S_i^-. Sometimes combinations out of multiple parameters are taken, too. One can think of the PDFs as the "behavior of the global χ^2 function in the neighborhood of the minimum". Obtained by diagonalization of the Hessian matrix when fitting a PDF [Pum+02]. In the code it is realized as:

```
75 def sigmaNC_unc(sign, pdfs, Q2, x, s):
76     """
77     Doc same to sigmaNC, but
78     :param pdfs: PDFSet()   List of PDF(). First one as central one
79                             and then pairwise eigenvector pdfs
80     :return:     ufloat     neutral current cross section with uncertainties
81     """
82     sigmas = []
83     for i in arange(1, len(pdfs), 2):
84         sigmas.append((sigmaNC(sign, pdfs[i], Q2, x, s)
85                        - sigmaNC(sign, pdfs[i + 1], Q2, x, s)) ** 2)
86     return uf(sigmaNC(sign, pdfs[0], Q2, x, s), sqrt(sum(sigmas)) / 2)
87
88 def sigmaCC_unc(sign, pdfs, Q2, x, s): # doc same as sigmaNC_unc() but for ch. current
89     sigmas = []
90     for i in arange(1, len(pdfs), 2):
91         sigmas.append((sigmaCC(sign, pdfs[i], Q2, x, s)
92                        - sigmaCC(sign, pdfs[i + 1], Q2, x, s)) ** 2)
93     return uf(sigmaCC(sign, pdfs[0], Q2, x, s), sqrt(sum(sigmas)) / 2)
```

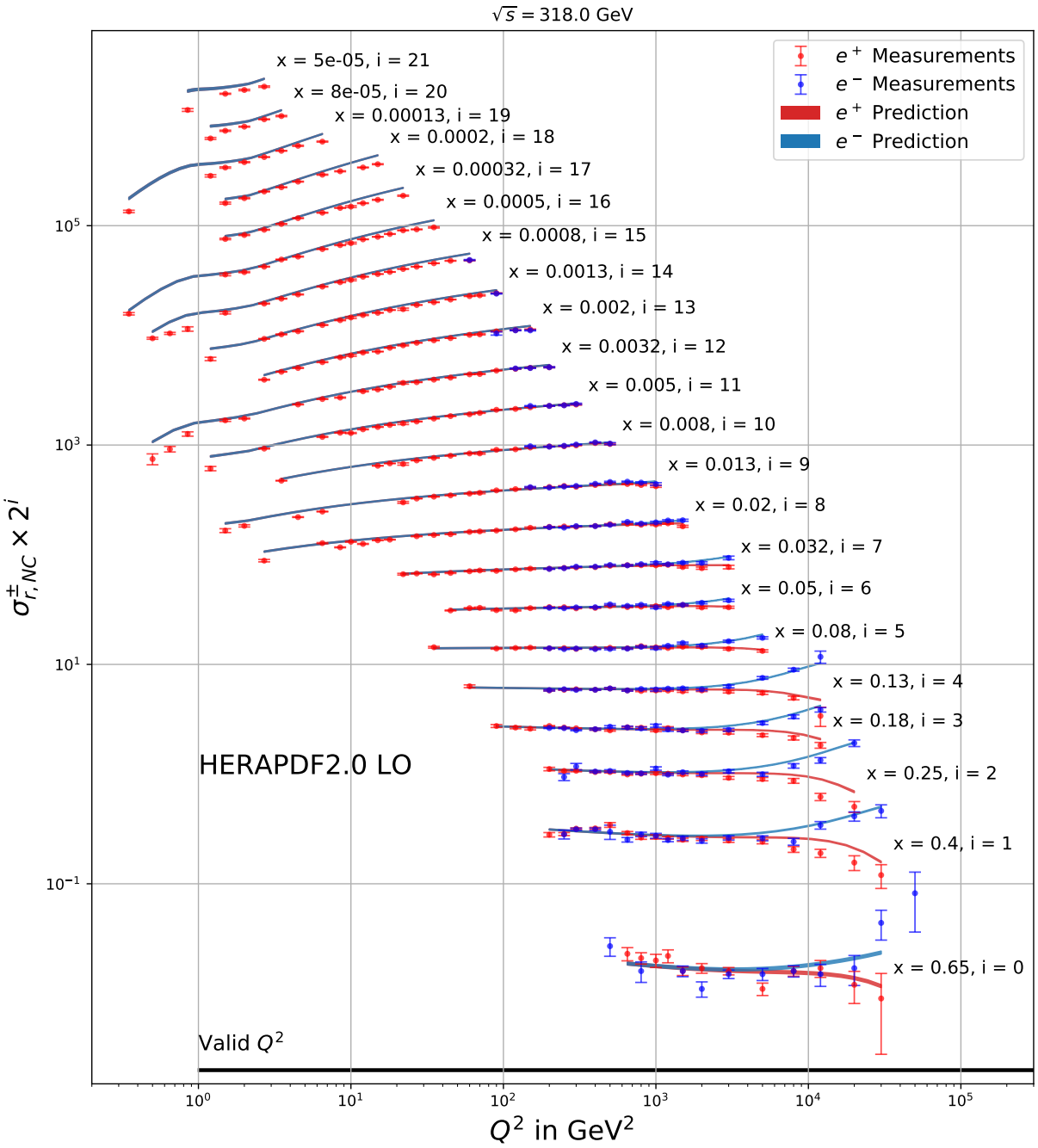

Figure 6: Neutral current reduced cross section for e^+ (red) and e^- (blue). Measurements with error bars and the prediction using HERAPDF20_LO_EIG as error bands. To separate different x, everything is stretched by 2^i and plotted logarithmically. The interval of valid Q^2 is drawn in the bottom.

4.2. Neutral Current

In Fig. 6 we show the $\sigma^{\pm}_{\mathrm{r,\,NC}}$ data compared to the prediction calculated with the HERAPDF20_LO_EIG fit. If there are no more than at least four data points that have x in common, we leave them out

in the plots. This is in order for a better perceptibility and less cluttering. The measured HERA data compared to numbers from our calculation with the HERAPDF20_LO_EIG, in Fig. 6, match well, when observed by the eye. For shrinking x below 0.008 or Q^2 below $10\,\mathrm{GeV}^2$ the discrepancy between calculated and measured data grows. Of course, this can be expected to happen below the valid Q^2 of $1\,\mathrm{GeV}^2$, but the trend starts already before. The same is true for $x > 0.13$ and for $Q^2 > 10^3\,\mathrm{GeV}^2$. One reason for the deviation is that our calculation is only done at tree level. Data is an all order prediction. Another more striking reason is that the patron densities $xf_q(x)$ only depend on x itself, but not Q^2 in our calculation. This explains a deviation at marginal values of x, Q^2, and both. A shortcoming of the prediction is the small uncertainties at the points where the HERA data has more variation or is scattering more. The prediction does not resemble the variation of the cross section at these points and should have a bigger uncertainty in the patron density functions.

When looking at the oldest PDF we'll compare to CTEQ6 in Fig. 7, a bigger uncertainty is immediately visible. Also, the deviation for smaller Q^2 and x deviates in the other direction than the HERA 2.0 Predictions go. A reason for this can be the different data set CTEQ6 uses. Also, the group in [Pum+02] did not have measurements at that low Q^2 as the predictions go to. For Q^2 under the valid Q^2 as given from CTEQ6, uncertainties expand. This is desirable as opposed to the behavior of HERA 2.0. For great x the two predictions agree with one another (except for $x = 0.4$).

With the CTEQs PDFs from 2010 we have drawn the predicted cross sections in Fig. 8. All characteristics from CTEQ6 hold for CT10, too. Only uncertainty has gone down and for low x the aberrance to the measurements shrank. This is due to the growing HERA-1 data which has become accessible leading up to CT10.

For CT18NNLO, part of the latest set CTEQ-TEA PDFs (2019), predictions are in Fig. 9. They created CT18NNLO using 28 different data sets, including the combined HERA data as the largest sets of all. For medium and greater x the behavior of the prediction has not changed to the eye. Only uncertainty has improved. But even so, HERA 2.0 claims to have smaller uncertainty than CT18NNLO. This is true for all marginal values of x and Q^2.

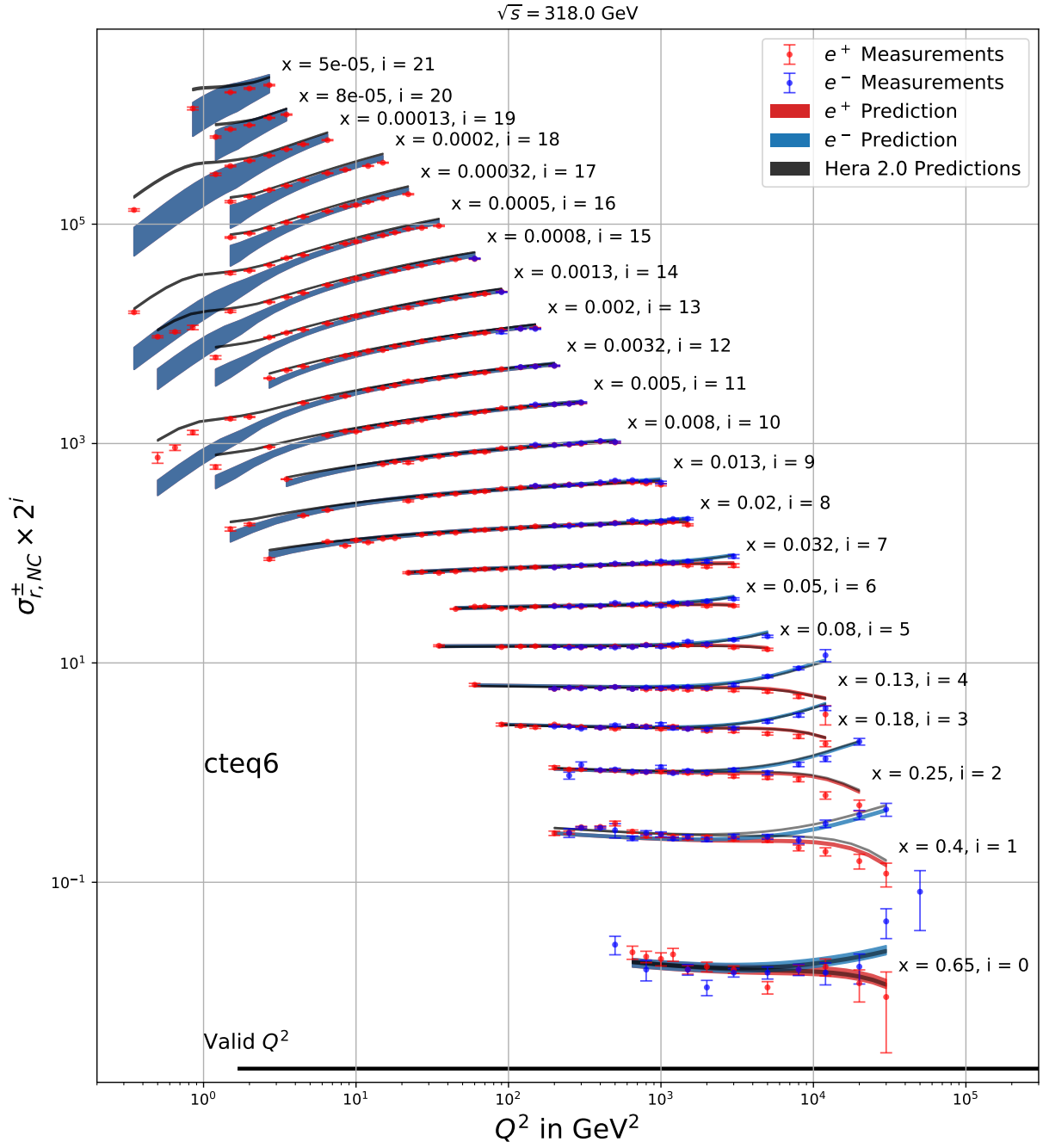

Figure 7: Comparison of neutral current reduced cross section with **CTEQ6** from 2002 for e^+ (red) and e^- (blue) and the HERA PDF in black. Measurements with error bars and the predictions as error bands. To separate different x, everything is stretched by 2^i and plotted logarithmically. The interval of valid Q^2 is drawn in the bottom.

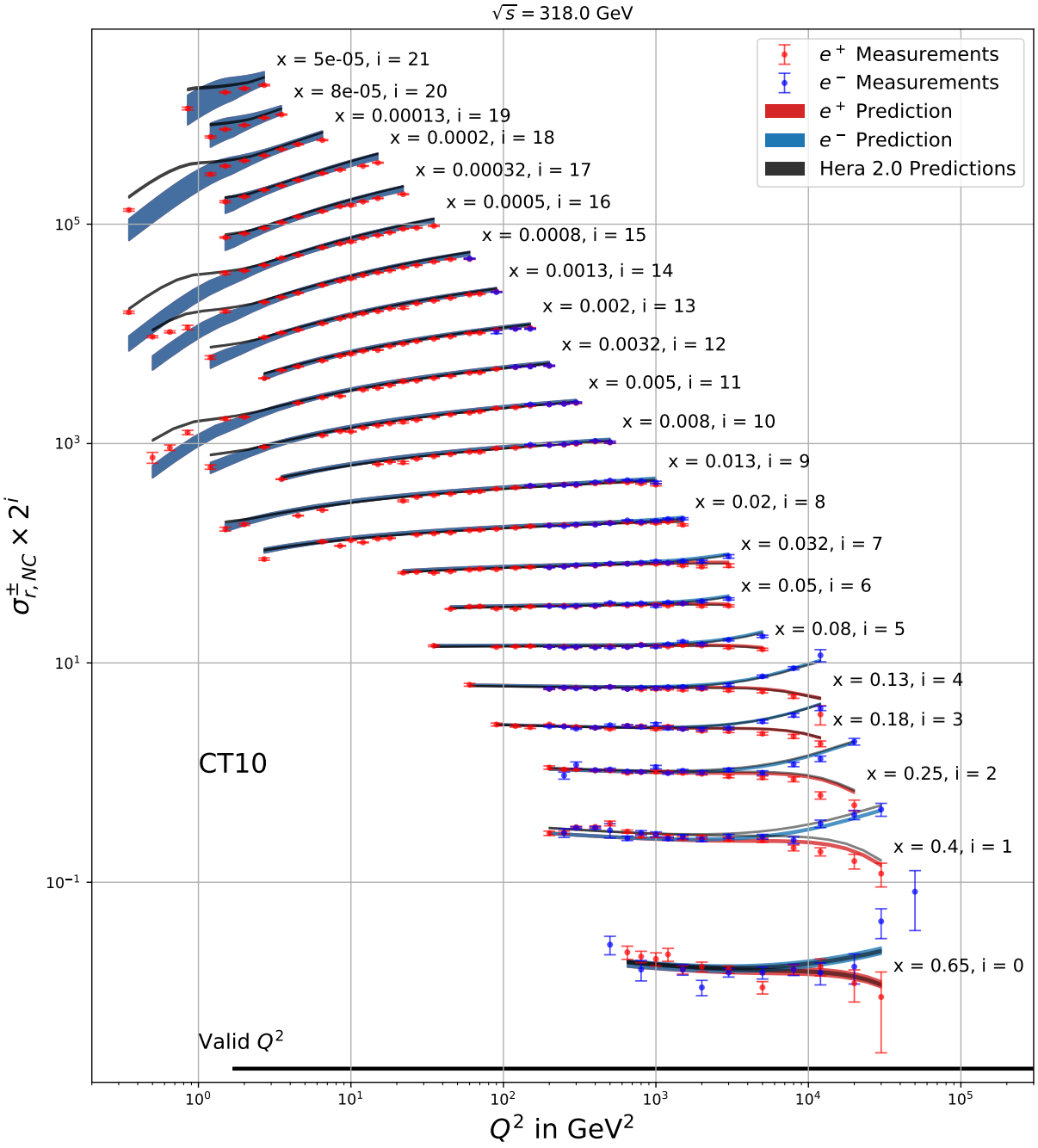

Figure 8: Comparison of neutral current reduced cross section with **CT10** from 2010 for e^+ (red) and e^- (blue) and the HERA PDF in black. Measurements with error bars and the predictions as error bands. To separate different x, everything is stretched by 2^i and plotted logarithmically. The interval of valid Q^2 is drawn in the bottom.

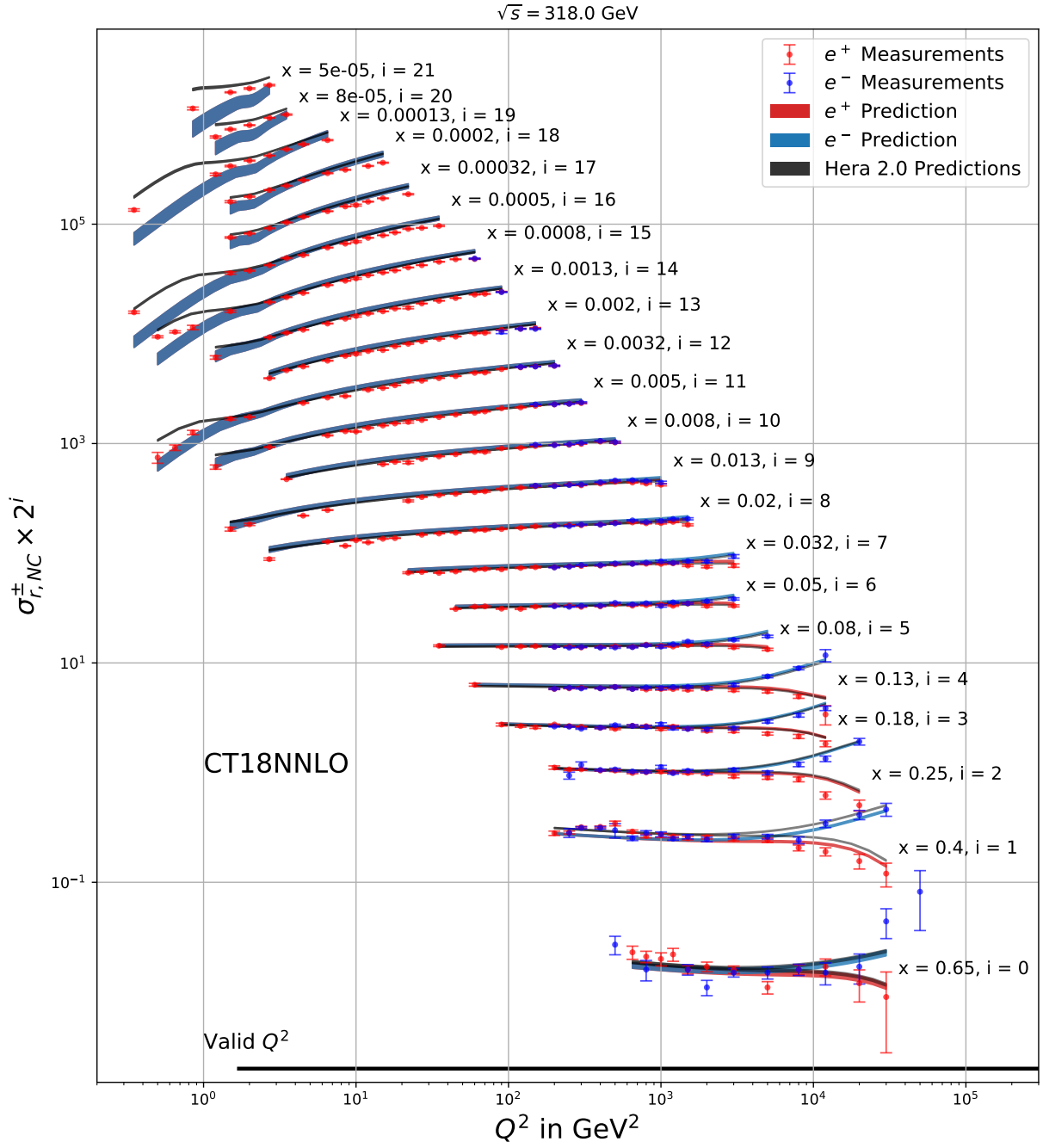

Figure 9: Comparison of neutral current reduced cross section with **CT18NNLO** from 2019 for e^+ (red) and e^- (blue) and the HERA PDF in black. Measurements with error bars and the predictions as error bands. To separate different x, everything is stretched by 2^i and plotted logarithmically. The interval of valid Q^2 is drawn in the bottom.

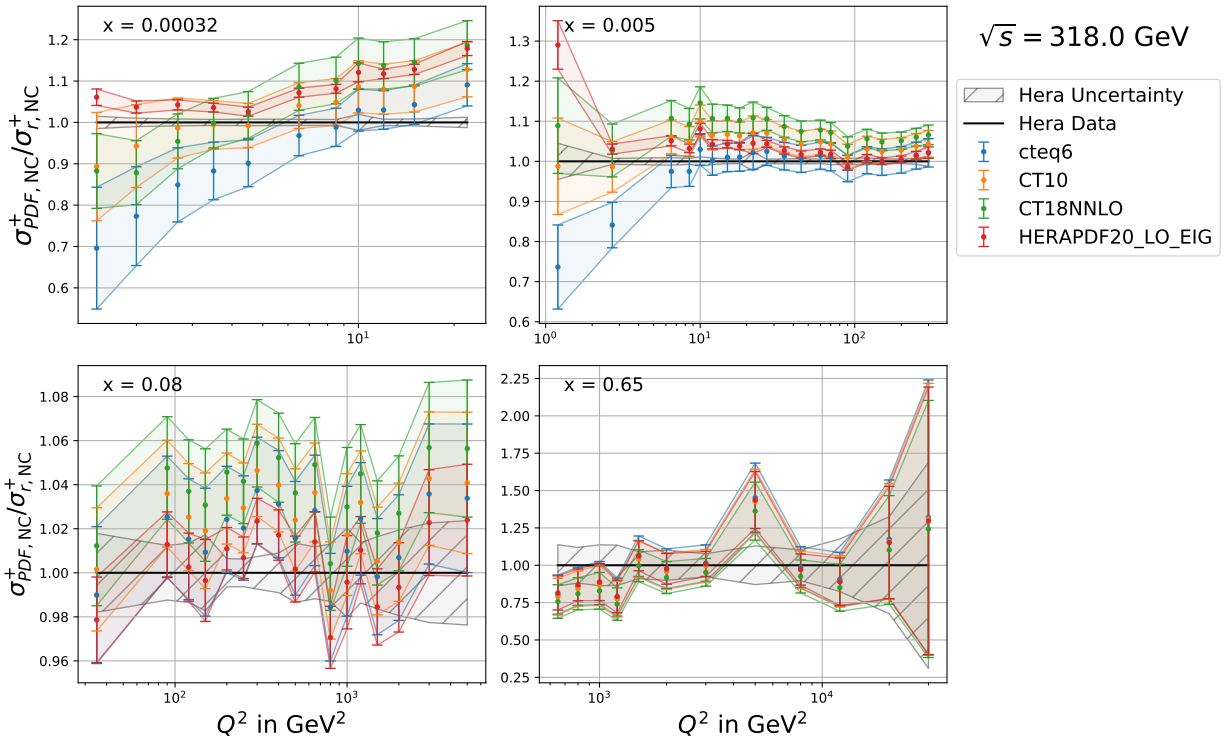

Figure 10: e^+: Ratios between predicted neutral current reduced cross section σ^+_{PDF}, calculated with the four PDFs, and the measurements σ^+_{NC}, for a selection of Bjorken x. Between the data points, uncertainty is joined linearly.

For a better view, we computed ratios between the measurements and predictions. To distinguish between the four PDFs we compare them for e^- in Fig. 11 and e^+ in Fig. 10. When dealing with small x as 0.000 32 in Fig. 10 the scattering is great and has a drift, compared to the rest. Farther, it should be noted that the scales of the ratios differ between the subplots. Again, for marginal Q^2 uncertainty grows (bottom right, Fig. 10) or the PDFs spread and leave the error band of the measured value (top both, Fig. 10). Also, in both subplots in top ($x = 0.000\,32$ and $x = 0.005$, Fig. 10) the error of HERA 2.0 PDF is significantly smaller than the error bands from CTEQ PDFs. This is to a degree that often predictions with CTEQ PDFs agree in the error bands with the measured value, but the HERA 2.0 PDF not.

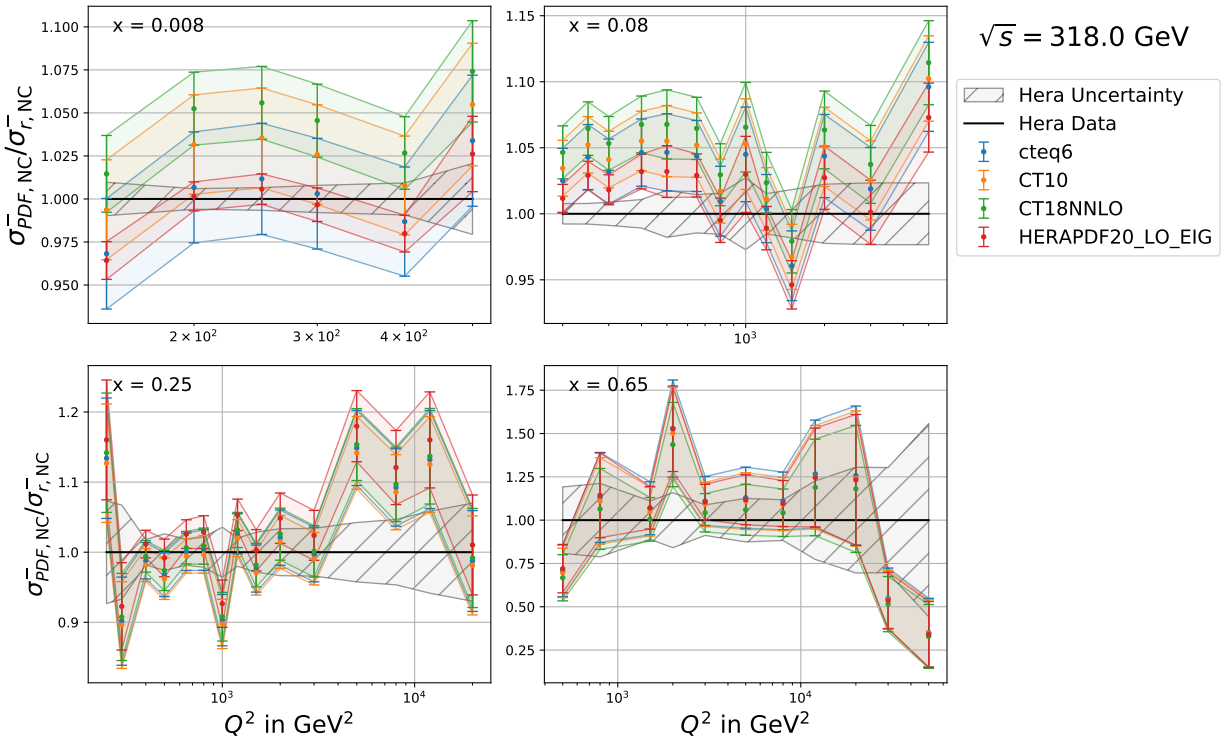

Figure 11: e^-: Ratios between predicted neutral current reduced cross section σ^-_{PDF}, calculated with the four PDFs, and the measurements σ^-_{NC}, for a selection of Bjorken x. Between the data points, uncertainty is joined linearly.

The ratios with the incoming electron e^- behave similarly (Fig. 11). The differences in predicted $\sigma^{\pm}_{\mathrm{NC}}$ only show up for Q^2 growing over at least $10^3\,\mathrm{GeV}^2$ (Fig. 6).

4.3. Charged Current

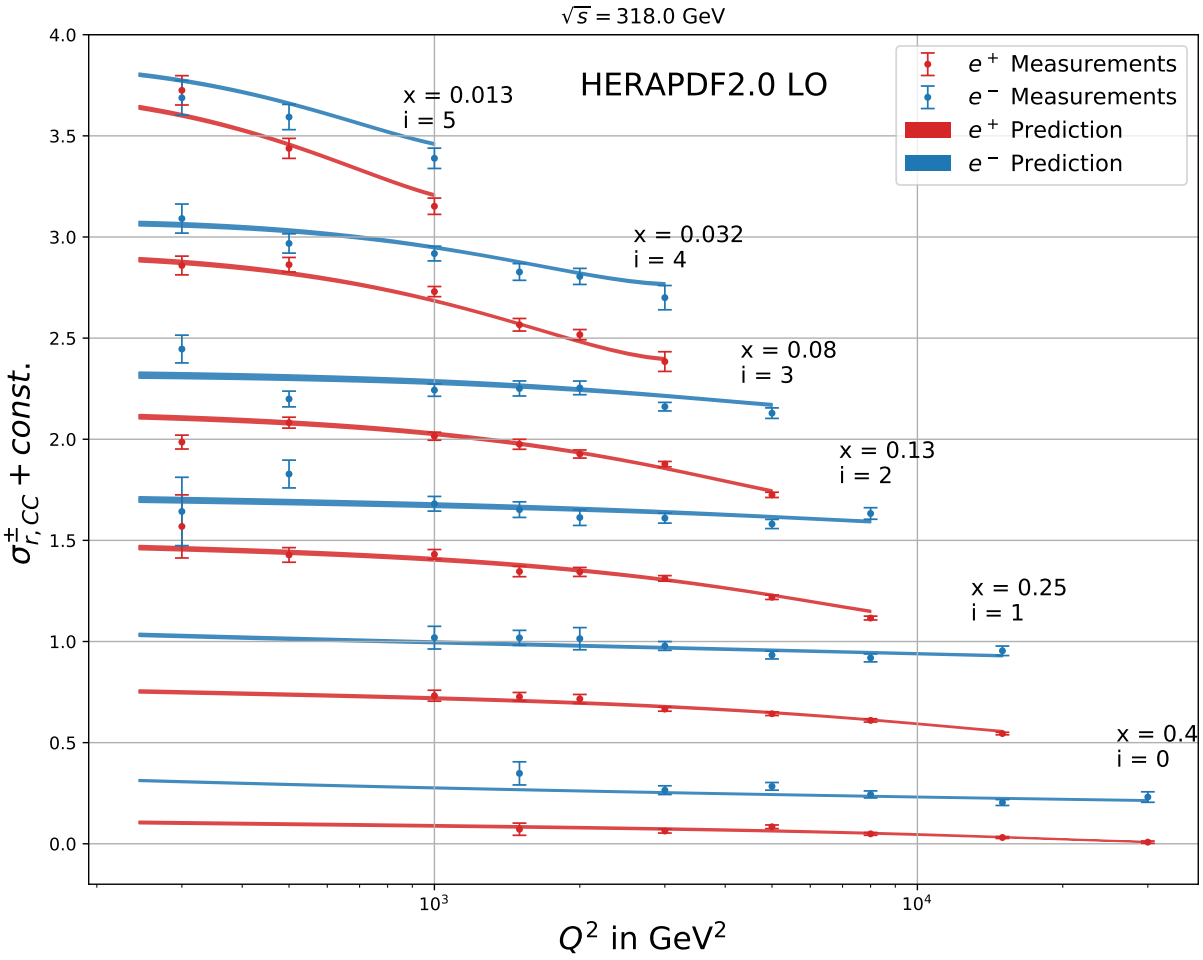

Figure 12: Charged current reduced cross section for e^+ (red) and e^- (blue). Measurements with error bars and the prediction using HERAPDF20_LO_EIG as error bands. To separate different x, the cross sections are each shifted.

A similar trend continues for the charged current reduced cross section. The prediction with HERA 2.0 PDF is displayed in Fig. 12. It again resembles the rough course of the measured data, but with errors that do not match with every error bar.

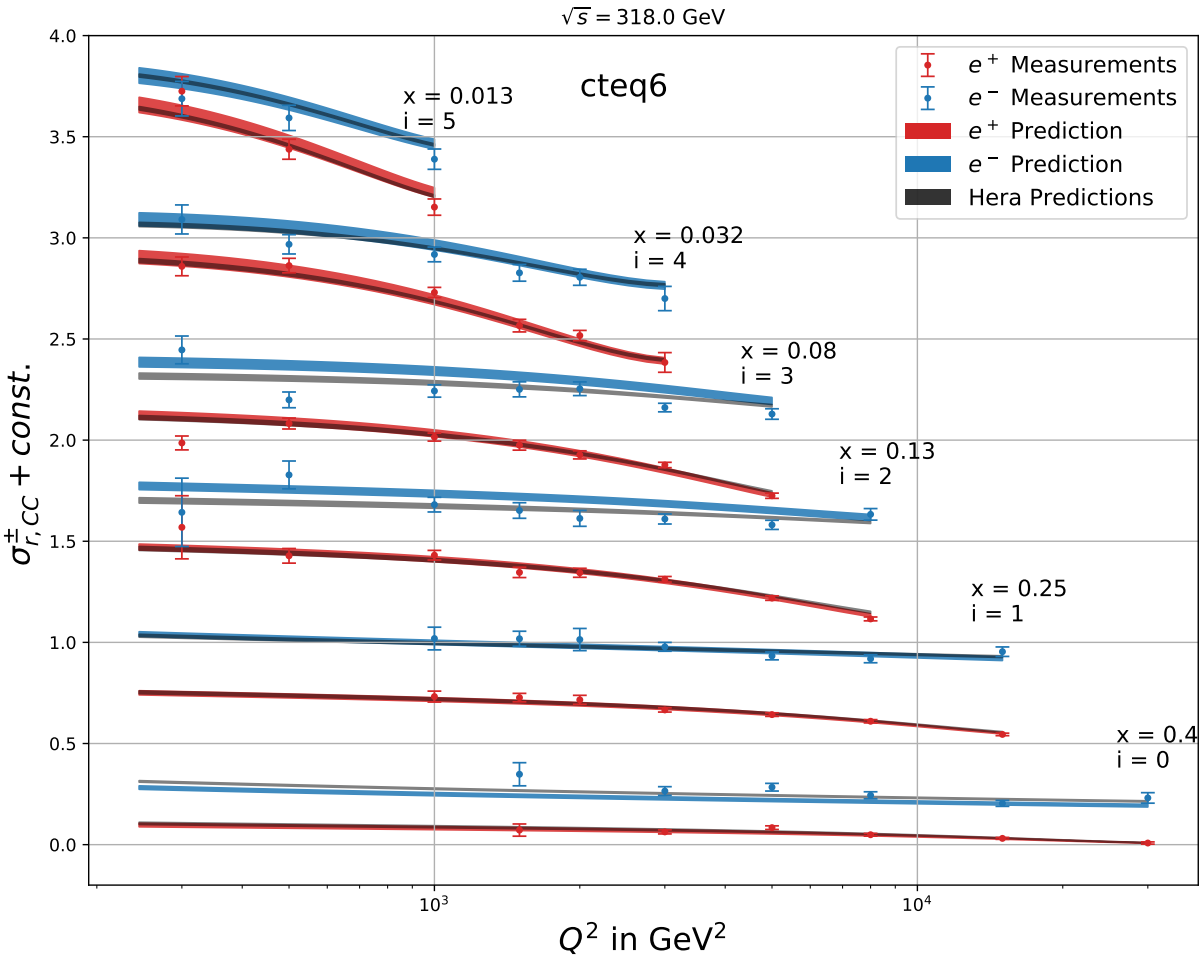

Figure 13: Comparison of charged current reduced cross section with **CTEQ6** from 2002 for e^+ (red) and e^- (blue) and the HERA PDF in black. Measurements with error bars and the predictions as error bands. To separate different x, the cross sections are each shifted.

Starting with CTEQ6, the prediction with greater errors already better fits the measurements, as seen in Fig. 13. Both agree in their error intervals, mostly.

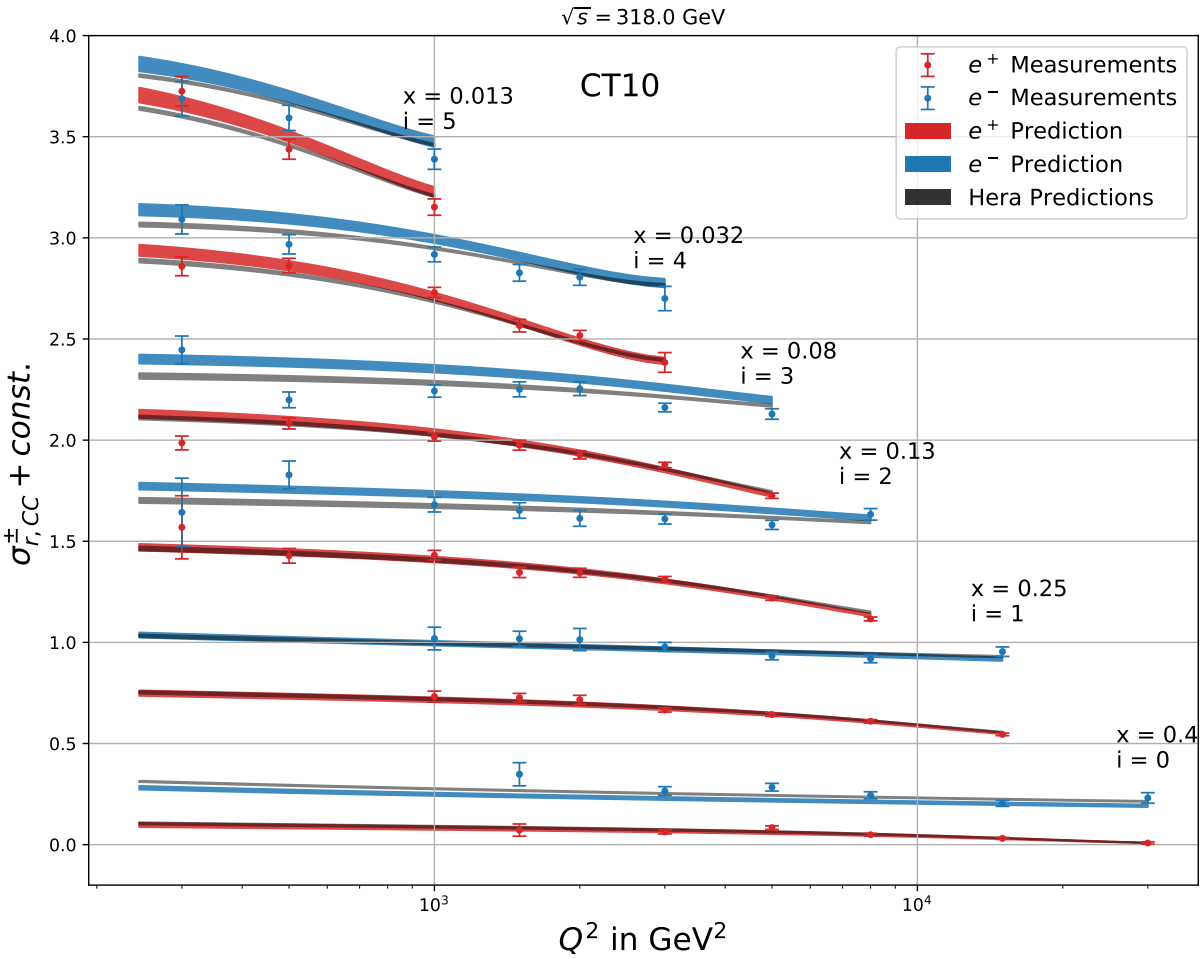

Figure 14: Comparison of charged current reduced cross section with **CT10** from 2010 for e^+ (red) and e^- (blue) and the HERA PDF in black. Measurements with error bars and the predictions as error bands. To separate different x, the cross sections are each shifted.

CT10 PDF brings the prediction to a deviation in higher cross sections, so that the errors start to not overlap with the prediction using HERA 2.0. This effect is greater for the two lowest x (Fig. 14).

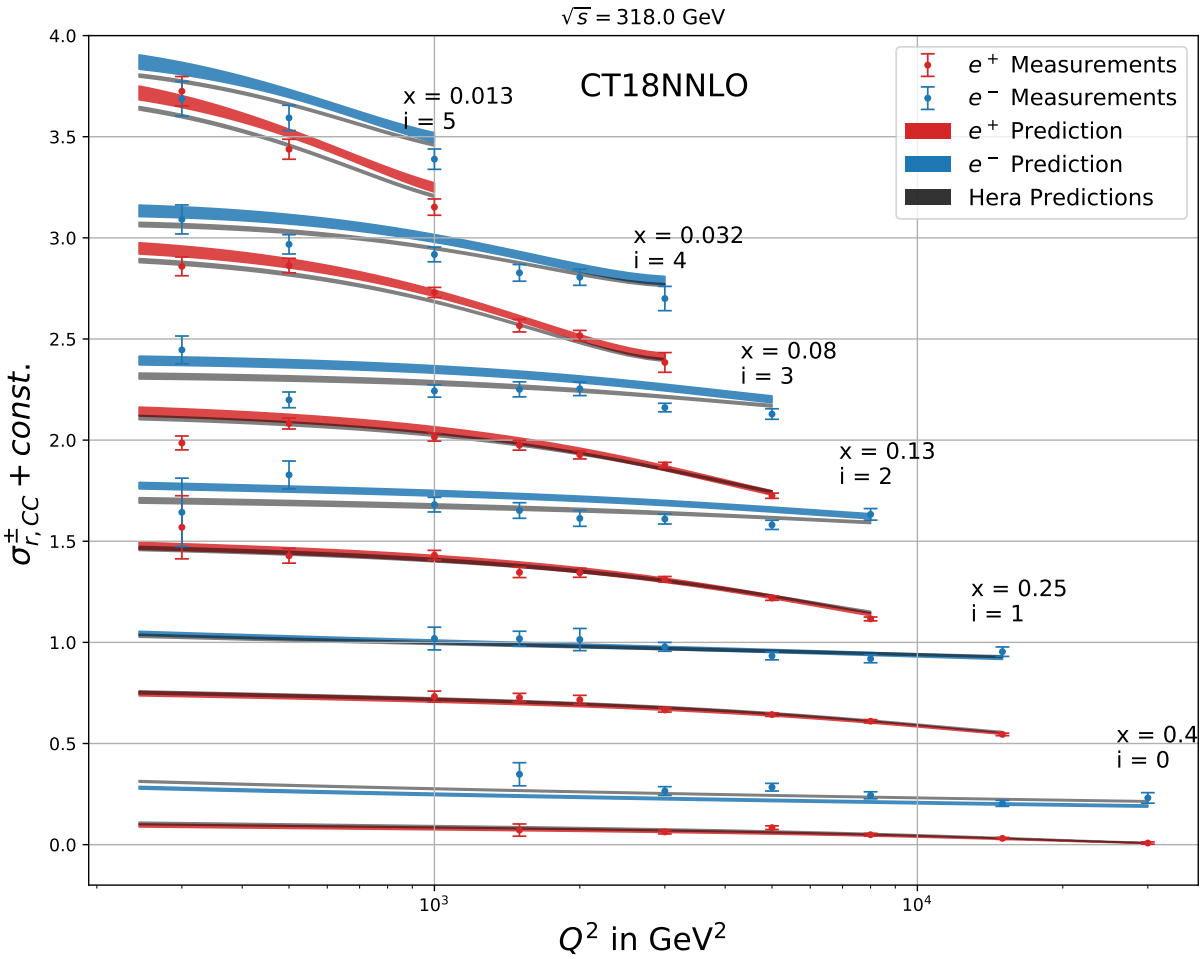

Figure 15: Comparison of charged current reduced cross section with **CT18NNLO** from 2019 for e^+ (red) and e^- (blue) and the HERA PDF in black. Measurements with error bars and the predictions as error bands. To separate different x, the cross sections are each shifted.

With the current CT18NNLO PDF the trend continues and more predictions have non-overlapping error bands (Fig. 15). With the ratios in Figs. 16a and 16b the trend becomes more clear. Over the years the CTEQ PDFs depart from HERA 2.0 PDF, while still agreeing with the measured data in the errors, for most of the data points. If someone wouldn't know that CTEQ takes other experiments into account, this should be the point of realization. Other, not displayed data sets pull the prediction to themselves. Most of the other data sets measure different physical phenomena [Hou+19, tab. 1].

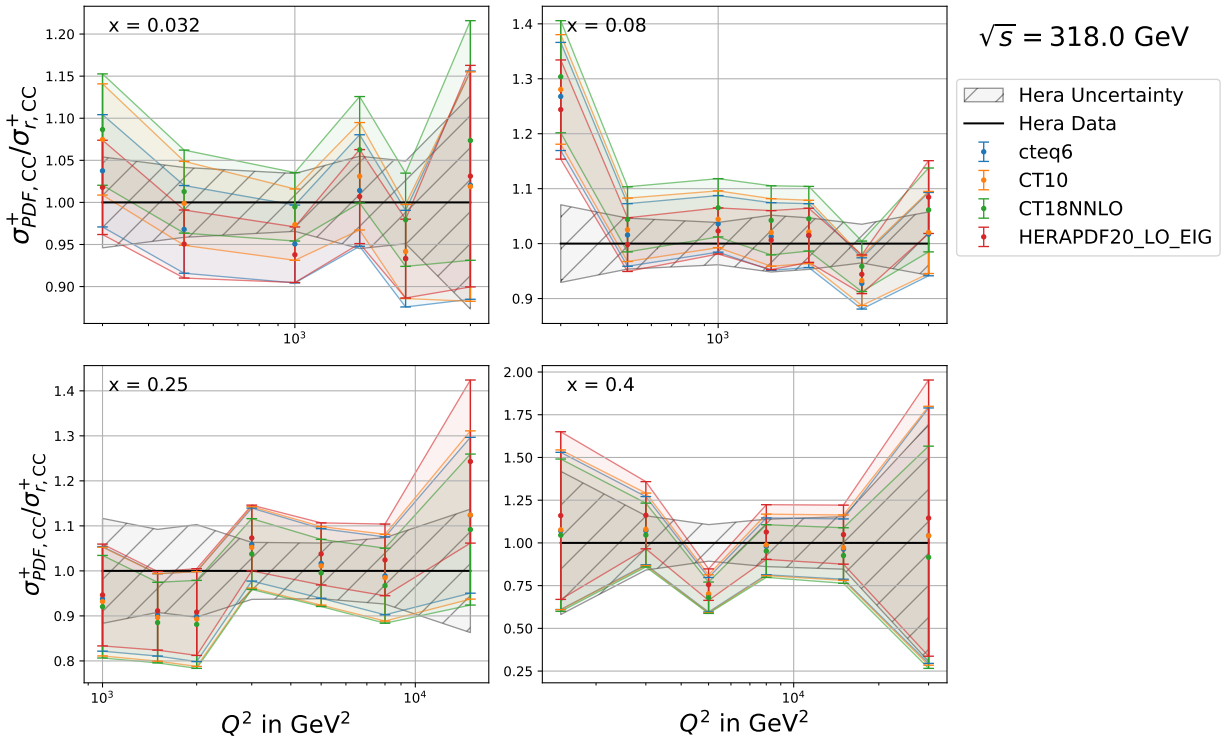

(a) e^+

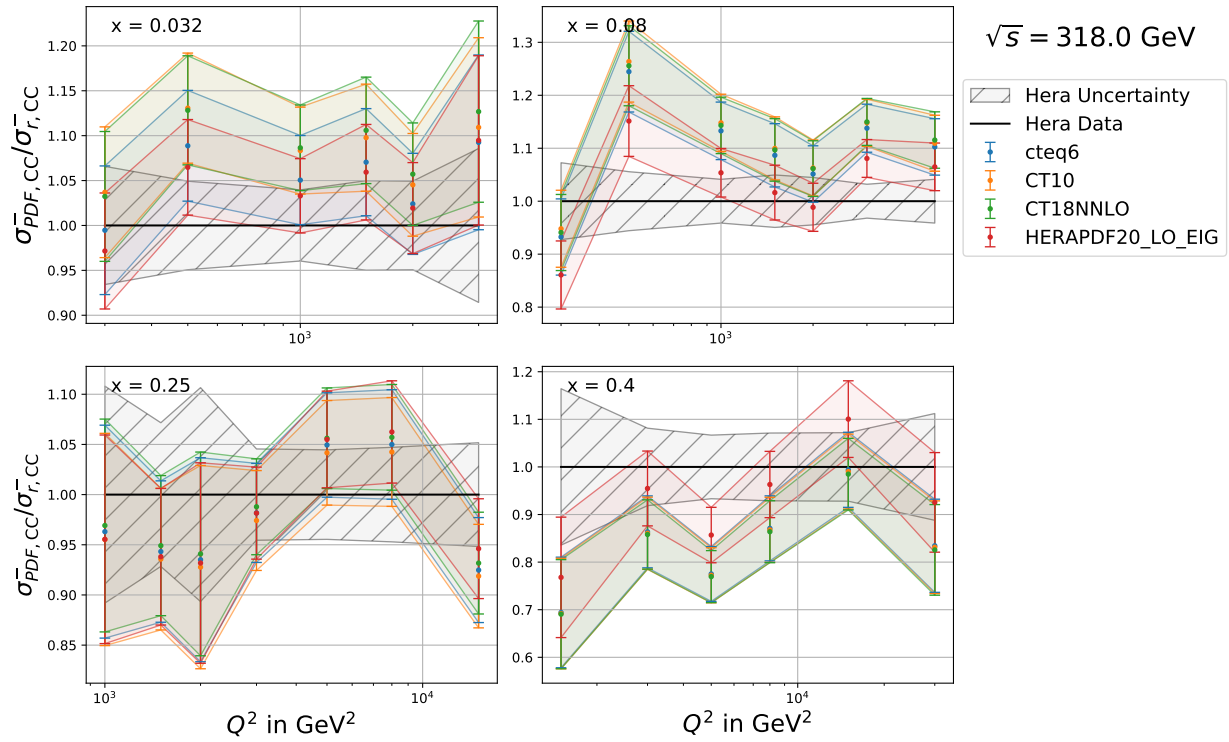

(b) e^-

Figure 16: Ratios between predicted charged current reduced cross section $\sigma^{\pm}_{\mathrm{PDF}}$, calculated with the four PDFs, and the measurements $\sigma^{\pm}_{\mathrm{CC}}$, for a selection of Bjorken x. Between the data points, uncertainty is joined linearly.

5. Summary

Within this bachelor's thesis, the goal was to compute the cross section of $e^{\pm}p$ scattering and observe the development of PDFs over time. First, $e^{-}\mu^{-}$ we calculated scattering in-depth with γ and Z boson exchange and interference, to get a taste of the workflow from the Feynman diagram to Lorentz invariant amplitude. We could facilitate the gained knowledge to see what $e^{-}q$ results in. After this overview, a generalized leptonic tensor was computed to speed up the process of calculating an invariant amplitude. Before e^{+} was missing and with the generalized leptonic tensor also the W boson exchange was easily done. $e^{\pm}q$ scattering for charged and neutral current has been solved, the parton model was the answer to the $e^{\pm}p$ process. After converting the invariant amplitude $\mathcal{M}$ into a differential cross section $\frac{\mathrm{d}^2\sigma^{e^{\pm}p}}{\mathrm{d}x\,\mathrm{d}Q^2}$, the solution could be compared. The H1 and ZEUS collaborations had data to compare to. Numerical implementation into Python then allowed using LHAPDF6, a straightforward way to calculate a prediction of the reduced cross sections. Three PDF sets of CTEQ that span a range from 2002 to 2019 and HERA 2.0 PDF have been used to analyze the cross section. One observation was that the HERA 2.0 PDF produced errors that did not resemble the uncertainty of their data. A trend over the years of CTEQ PDFs is shrinking errors, although they do not fall under the too-small uncertainties of the HERA 2.0 PDF. This is a sign of a healthy improvement. An outlook for a further advance is incorporating more orders of Feynman diagrams to improve the precision of prediction.

A. Dirac Algebra

For the calculations presented in this thesis, we need the Dirac spinor algebra. In the following section the used Lorentz invariant notation is presented and stated [Ili16; Zee10].

A.1. Dirac Matrices

Starting of with the Dirac equation

$$(i\not{\partial} - m)\,\psi(x) = 0, \tag{A.1}$$

that already introduces the notation $\not{\partial} := \gamma^\mu \partial_\mu$, leads to the γ^μ Dirac matrices. The γ^μ satisfy the Clifford algebra $\mathrm{Cl}_4(\mathbb{R})$

$$\frac{1}{2}\{\gamma^\mu, \gamma^\nu\} = \frac{1}{2}(\gamma^\mu\gamma^\nu + \gamma^\nu\gamma^\mu) = g^{\mu\nu}\mathbb{1}_4, \qquad \gamma^{\mu\dagger} = \gamma^0\gamma^\mu\gamma^0. \tag{A.2}$$

$$\Rightarrow \left(\gamma^0\right)^2 = -(\gamma^\eta)^2 = \mathbb{1}_4, \qquad \gamma^{0\dagger} = \gamma^0, \quad \gamma^{\eta\dagger} = -\gamma^\eta \tag{A.3}$$

where $\mu, \nu \in 0, 1, 2, 3$, $\eta \in 1, 2, 3$ and $\mathbb{1}_4$ is the identity matrix. When asking how a Dirac spinor ψ transforms, another matrix, namely γ^5, can be constructed. The only possible product is

$$\gamma^5 = i\gamma^0\gamma^1\gamma^2\gamma^3 = -\frac{i}{4}\epsilon_{\mu\nu\alpha\beta}\gamma^\mu\gamma^\nu\gamma^\alpha\gamma^\beta \tag{A.4}$$

with the convention of $\epsilon^{0123} = -\epsilon_{0123} = 1$. It isn't called γ^4 because of the historical notation of time as the fourth dimension[5]. Useful relations arise from this, especially

$$\left(\gamma^5\right)^2 = \gamma^5, \qquad \gamma^{5\dagger} = \gamma^5 \quad \text{and} \quad \{\gamma_5, \gamma^\mu\} = 0. \tag{A.5}$$

Also interesting in $\mathrm{Cl}_4(\mathbb{R})$ are

$$\gamma^\mu\gamma_\mu = 4\,\mathbb{1}_4, \qquad \gamma^\mu\gamma^\nu\gamma_\mu = -2\gamma^\nu, \qquad \epsilon^{\alpha\beta\mu\nu}\epsilon_{\alpha\beta\sigma\rho} = 2\Big(\delta^\mu_\rho\delta^\nu_\sigma - \delta^\mu_\sigma\delta^\nu_\rho\Big). \tag{A.6}$$

δ is the Kronecker delta for which $g_{ab}g^{bc} = \delta^c_a$ holds. Other relations: [Nag13b]

$$\begin{aligned} \gamma_\mu \not{A}\gamma^\mu &= -2\not{A} & \gamma_\mu \not{A}\not{B}\not{C}\gamma^\mu &= -2\not{C}\not{B}\not{A} \\ \gamma_\mu \not{A}\not{B}\gamma^\mu &= 4(A\cdot B) & \gamma_\mu \not{A}\not{B}\not{C}\not{D}\gamma^\mu &= 2(\not{D}\not{A}\not{B}\not{C} - \not{C}\not{B}\not{A}\not{D}) \end{aligned} \tag{A.7}$$

Plane wave solutions of Eq. (A.1) are [Nag13a]

$$u_r(p) = \begin{bmatrix} \sqrt{p\cdot\sigma}\xi_r \\ \sqrt{p\cdot\bar{\sigma}}\xi_r \end{bmatrix} = \sqrt{\frac{E+m}{2}} \begin{bmatrix} \left(1 - \frac{\sigma\cdot p}{E+m}\right)\xi_r \\ \left(1 + \frac{\sigma\cdot p}{E+m}\right)\xi_r \end{bmatrix} \tag{A.8}$$

[5] Zee10, "The peculiar name comes about because in some old-fashioned notation the time coordinate was called x^4 with a corresponding γ^4." p.95.

$$v_r(p) = \begin{bmatrix} \sqrt{p\cdot\sigma}\eta_r \\ -\sqrt{p\cdot\bar{\sigma}}\eta_r \end{bmatrix} = \sqrt{\frac{E+m}{2}} \begin{bmatrix} \left(1 - \frac{\sigma\cdot p}{E+m}\right)\eta_r \\ -\left(1 + \frac{\sigma\cdot p}{E+m}\right)\eta_r \end{bmatrix} \tag{A.9}$$

$$\xi_1 = \begin{bmatrix} 1 \\ 0 \end{bmatrix}, \quad \xi_2 = \begin{bmatrix} 0 \\ 1 \end{bmatrix}, \quad \eta_r = i\sigma_2\xi_r^* = \begin{bmatrix} 0 & 1 \\ -1 & 0 \end{bmatrix}\xi_r^* \tag{A.10}$$

and when summing over polarization, lead us to the completeness relations for particles u and antiparticles v

$$\sum_{r=\pm 1/2} u_r\bar{u}_r(p) = \not{p} + m, \qquad \sum_{r=\pm 1/2} v_r\bar{v}_r(p) = \not{p} - m. \tag{A.11}$$

A.2. Trace Theorems

For fermionic matrix elements it is near about mandatory to calculate traces of Dirac matrices. The most basic and useful trace theorems for matrices are

$$\mathrm{tr}(A) = \mathrm{tr}\left(A^T\right), \qquad \mathrm{tr}(A+B) = \mathrm{tr}(A) + \mathrm{tr}(B), \qquad \mathrm{tr}(A_1 \dots A_N) = \mathrm{tr}(A_N A_1 \dots A_{N-1}). \tag{A.12}$$

But what can we gain in terms of γ matrices? The first consequence is that $\mathrm{tr}\left(\gamma^\mu\gamma^\nu\right) = g^{\mu\nu}\,\mathrm{tr}(\mathbb{1}) = 4g^{\mu\nu}$. γ^5 is anticommutative and $\left(\gamma^5\right)^2 = \mathbb{1}$ so

$$\begin{aligned} \mathrm{tr}\left(\gamma^{\nu_1}\cdots\gamma^{\nu_n}\right) &= \mathrm{tr}\left(\gamma^{\nu_1}\cdots\gamma^{\nu_n}\gamma^5\gamma^5\right) \\ &= \mathrm{tr}\left(\gamma^5\gamma^{\nu_1}\cdots\gamma^{\nu_n}\gamma^5\right) \\ &= (-1)^n\,\mathrm{tr}\left(\gamma^{\nu_1}\cdots\gamma^{\nu_n}\gamma^5\gamma^5\right) \\ &= (-1)^n\,\mathrm{tr}\left(\gamma^{\nu_1}\cdots\gamma^{\nu_n}\right), \end{aligned} \tag{A.13}$$

meaning any trace with an odd number of γ matrices (excluding γ^5) vanishes: 0. For four γ matrices

$$\begin{aligned} \mathrm{tr}\left(\gamma^\delta\gamma^\mu\gamma^\eta\gamma^\nu\right) &= \mathrm{tr}\left(\gamma^\mu\gamma^\eta\gamma^\nu\gamma^\delta\right) \\ &= -\,\mathrm{tr}\left(\gamma^\mu\gamma^\eta\gamma^\delta\gamma^\nu\right) + 2g^{\delta\nu}\,\mathrm{tr}\left(\gamma^\mu\gamma^\eta\right) \\ &= -\,\mathrm{tr}\left(\gamma^\mu\gamma^\eta\gamma^\delta\gamma^\nu\right) + 8g^{\delta\nu}g^{\mu\eta} \\ &= \mathrm{tr}\left(\gamma^\mu\gamma^\delta\gamma^\eta\gamma^\nu\right) - 8g^{\eta\delta}g^{\mu\nu} + 8g^{\delta\nu}g^{\mu\eta} \\ &= -\,\mathrm{tr}\left(\gamma^\delta\gamma^\mu\gamma^\eta\gamma^\nu\right) + 8g^{\delta\mu}g^{\eta\nu} - 8g^{\eta\delta}g^{\mu\nu} + 8g^{\delta\nu}g^{\mu\eta}, \end{aligned} \tag{A.14}$$

so $\mathrm{tr}\left(\gamma^\delta\gamma^\mu\gamma^\eta\gamma^\nu\right) = 4\left(g^{\delta\mu}g^{\eta\nu} - g^{\delta\eta}g^{\mu\nu} + g^{\delta\nu}g^{\mu\eta}\right)$.
$\mathrm{tr}\left(\gamma^\delta\gamma^\mu\gamma^\eta\gamma^\nu\gamma^5\right) = -4i\epsilon^{\delta\mu\eta\nu}$, because of the anticommutative behavior, a permutation of the γ's changes the sign of the trace. This means it must be proportional to $\epsilon^{\delta\mu\eta\nu}$. The constant $-4i$ can

directly be calculated. Also

$$\mathrm{tr}(\gamma^\mu\gamma^\mu) = 16 \qquad \text{and} \qquad \mathrm{tr}(\gamma_5\gamma^\mu\gamma^\nu) = 0. \tag{A.15}$$

A.3. Chirality

It is useful to be able to decompose a Dirac field ψ into a left-handed and a right-handed part $\psi = \psi_L + \psi_R$. Helicity is a freedom a particle has. It describes the direction of spin. In particle interaction, a vertex factor as shown shortly can act on both parts differently. The physics of the Dirac equation Eq. (A.1) still has to be independent of the chosen basis. The solution to this are the chiral projection operators $P_L := \frac{1}{2}(1-\gamma^5)$ and $P_R := \frac{1}{2}(1+\gamma^5)$ for which $\psi_L = P_L\psi$ and $\psi_R = P_R\psi$.

$$P_{L/R}^2 = \frac{1}{4}\left(1 \mp 2\gamma^5 + \left(\gamma^5\right)^2\right) = \frac{1}{2}\left(1 \mp \gamma^5\right) = P_{L/R} \qquad \text{and} \qquad P_L P_R = \frac{1}{4}\left(1 - \left(\gamma^5\right)^2\right) = 0 \tag{A.16}$$

This symmetry corresponds to the conservation of axial current [Zee10, pp. 98].

A.4. Feynman Rules

To evaluate a process, one has to draw all diagrams that are topologically different. Every element of a diagram has a factor as given in the following Appendices A.4.1 to A.4.3. To gain a Lorentz-invariant scattering amplitude $\mathcal{M}$, we multiply together these factors. The order of multiplication starts with an outgoing fermion particle, identifiable by a straight line with an arrow representing particle flow on top, and vertex factors in between. The propagator factors connect these particle factors [HM84; Nag13b].

We only need to look once at topologically same diagrams, because Feynmans approach to interactions integrates over the temporal component. Here it makes no difference whether the propagator first gets emitted or absorbed. We show this in Fig. 17. [Ohl11]

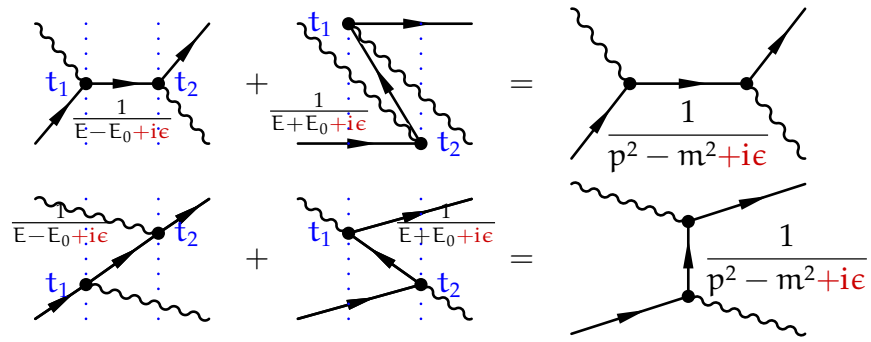

Figure 17: Visualization of the temporal indifference of topologically identical Feynman diagrams. [Ohl11, p. 19]

A.4.1. External Lines

This work only deals with in- and outgoing spin-$\frac{1}{2}$ particles. We read all diagrams from left to right, so we denote ingoing fermions as u, outgoing as $\overline{u}$, call ingoing antifermions $\overline{v}$, and outgoing ones v. Notice all four kinds in Fig. 18. The particles can have an assigned momentum.

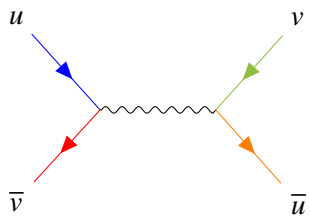

Figure 18: In- and outgoing fermions.

A.4.2. Internal Lines

Every internal line has an associated propagator to it, a fermion as well as a photon and W, Z boson. The propagators used in our calculation are written down in Fig. 19.

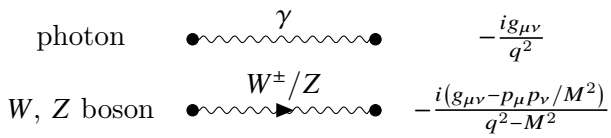

Figure 19: Propagators for the internal lines of the used vector bosons. q is the carried momentum and M the particle's mass.

A.4.3. Vertex Factors

The vertex factors read as in Fig. 20.

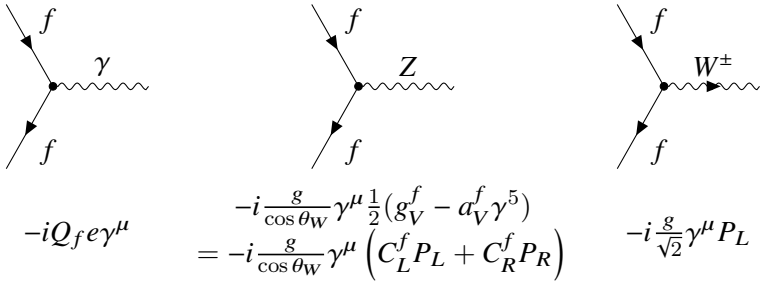

Figure 20: Vertex Factors with $g=\frac{e}{\sin\theta_W}$ and projection operators $P_{L/R}$. Q_f is the fermion's charge relative to the positron's. $C_{L/R}^f$ describe the amount of coupling for the corresponding helicity and g_V^f, a_V^f vector and axial vector couplings.

The total squared transition matrix $|\mathcal{M}|^2$ can be calculated, when all separate diagrams have been gathered and the invariant amplitudes $\mathcal{M}_i$ have been acquired. Finally

$$|\mathcal{M}|^2=\sum_i \mathcal{M}_i \times \sum_i \mathcal{M}_i^\dagger \tag{A.17}$$

When there are two different diagrams we get

$$|\mathcal{M}|^2 = |\mathcal{M}_1|^2 + |\mathcal{M}_2|^2 + 2\mathfrak{R}\Big(\mathcal{M}_1\mathcal{M}_2^\dagger\Big). \tag{A.18}$$

Lastly, the average over the possible polarizations has to be calculated to gain the unpolarized cross section, revealing $\overline{|\mathcal{M}|^2}$. For further insight they should examine the solution in Mandelstam variables.

References

[Buc+15] Andy Buckley et al. "LHAPDF6: parton density access in the LHC precision era". In: *Eur. Phys. J. C* 75 (2015), p. 132. DOI: 10.1140/epjc/s10052-015-3318-8. arXiv: 1412.7420 [hep-ph].

[Ell17] Joshua P. Ellis. "TikZ-Feynman: Feynman diagrams with TikZ". In: *Computer Physics Communications* 210 (2017), pp. 103–123. ISSN: 0010-4655. DOI: https://doi.org/10.1016/j.cpc.2016.08.019. arXiv: 1601.05437 [hep-ph]. URL: http://www.sciencedirect.com/science/article/pii/S0010465516302521.

[Fri91] Jerome I. Friedman. "Deep inelastic scattering: Comparisons with the quark model". In: *Rev. Mod. Phys.* 63 (3 July 1991), pp. 615–627. DOI: 10.1103/RevModPhys.63.615. URL: https://link.aps.org/doi/10.1103/RevModPhys.63.615.

[HM84] Francis Halzen and Alan D. Martin. *Quarks and Leptons: An Introductory Course in Modern Particle Physics*. John Wiley & Sons, Inc., 1984.

[Hou+19] Tie-Jiun Hou et al. "New CTEQ global analysis of quantum chromodynamics with high-precision data from the LHC". In: (Dec. 2019). arXiv: 1912.10053 [hep-ph].

[HZ15] H1 and ZEUS Collaborations. "Combination of Measurements of Inclusive Deep Inelastic $e^{\pm}p$ Scattering Cross Sections and QCD Analysis of HERA Data". In: *arXiv e-prints*, arXiv:1506.06042 (June 2015), arXiv:1506.06042. arXiv: 1506.06042 [hep-ex].

[Ili16] Victor Ilisie. "Dirac Algebra". In: *Concepts in Quantum Field Theory: A Practitioner's Toolkit*. Cham: Springer International Publishing, 2016, pp. 69–84. ISBN: 978-3-319-22966-9. DOI: 10.1007/978-3-319-22966-9_5. URL: https://doi.org/10.1007/978-3-319-22966-9_5.

[Ken91] Henry W. Kendall. "Deep inelastic scattering: Experiments on the proton and the observation of scaling". In: *Rev. Mod. Phys.* 63 (3 July 1991), pp. 597–614. DOI: 10.1103/RevModPhys.63.597. URL: https://link.aps.org/doi/10.1103/RevModPhys.63.597.

[Kov] Karol Kovařík. "Deep inelastic scattering". In: *Hitchhiker's Guide to Renormalization*. Unpublished, Ver.1.4.

[Lai+10] Hung-Liang Lai et al. "New parton distributions for collider physics". In: *Phys. Rev. D* 82 (2010), p. 074024. DOI: 10.1103/PhysRevD.82.074024. arXiv: 1007.2241 [hep-ph].

[Mar94] A. D. Martin. "QCD and Deep Inelastic Scattering". In: *Addendum to the 1993 European School of High-Energy Physics*. Ed. by N. Ellis and Gavela M. B. CERN 94-04. Geneva: CERN, June 1994.

[Nag13a] Yorikiyo Nagashima. "Appendix A: Gamma Matrix Traces and Cross Sections". In: *Foundations of the Standard Model*. Elementary Particle Physics. Boschstr. 12, 69469 Weinheim, Germany: WILEY-VCH Verlag GmbH & Co. KGaA, Feb. 2013, pp. 501–506. ISBN: 9783527648887. DOI: 10.1002/9783527648887.app1. eprint: https://onlinelibrary.wiley.com/doi/pdf/10.1002/9783527648887.app1. URL: https://onlinelibrary.wiley.com/doi/abs/10.1002/9783527648887.app1.

[Nag13b] Yorikiyo Nagashima. "Appendix B: Feynman Rules for the Electroweak Theory". In: *Elementary Particle Physics*. Elementary Particle Physics. Boschstr. 12, 69469 Weinheim, Germany: WILEY-VCH Verlag GmbH & Co. KGaA, Feb. 2013, pp. 507–511. ISBN: 9783527648887. DOI: 10.1002/9783527648887.app2. eprint: https://onlinelibrary.wiley.com/doi/pdf/10.1002/9783527648887.app2. URL: https://onlinelibrary.wiley.com/doi/abs/10.1002/9783527648887.app2.

[Nag13c] Yorikiyo Nagashima. *Foundations of the Standard Model*. Elementary Particle Physics. Boschstr. 12, 69469 Weinheim, Germany: WILEY-VCH Verlag GmbH & Co. KGaA, Feb. 2013. ISBN: 9783527648887. DOI: 10.1002/9783527648887. URL: https://onlinelibrary.wiley.com/doi/book/10.1002/9783527648887.

[Ohl11] Thorsten Ohl. *Feynman Diagrams For Pedestrians*. Lecture proceeding. Sept. 2011. URL: http://www.pp.rhul.ac.uk/~kauer/projects/scripts/ohl.pdf.

[Ohl96] Thorsten Ohl. *feynmf – Macros and fonts for creating Feynman (and other) diagrams*. CTAN – Comprehensive TeX Archive Network. 1996. URL: https://ctan.org/pkg/feynmf.

[PDG+20a] PDG et al. "Monte Carlo Particle Numbering Scheme". In: vol. 2020. 8. 083C01. Aug. 2020, pp. 661–664. DOI: 10.1093/ptep/ptaa104. eprint: https://academic.oup.com/ptep/article-pdf/2020/8/083C01/33653179/ptaa104.pdf. URL: https://pdg.lbl.gov/2020/reviews/rpp2020-rev-monte-carlo-numbering.pdf.

[PDG+20b] PDG et al. "Review of Particle Physics". In: *Progress of Theoretical and Experimental Physics* 2020.8 (Aug. 2020). 083C01. ISSN: 2050-3911. DOI: 10.1093/ptep/ptaa104. eprint: https://academic.oup.com/ptep/article-pdf/2020/8/083C01/33653179/ptaa104.pdf. URL: https://doi.org/10.1093/ptep/ptaa104.

[Pum+02] J. Pumplin et al. "New generation of parton distributions with uncertainties from global QCD analysis". In: *JHEP* 07 (2002), p. 012. DOI: 10.1088/1126-6708/2002/07/012. arXiv: hep-ph/0201195.

[SMO20] Vladyslav Shtabovenko, Rolf Mertig, and Frederik Orellana. "FeynCalc 9.3: New features and improvements". In: *Computer Physics Communications* 256 (2020), p. 107478. ISSN: 0010-4655. DOI: https://doi.org/10.1016/j.cpc.2020.107478. arXiv: 2001.04407 [hep-ph]. URL: http://www.sciencedirect.com/science/article/pii/S001046552030223X.

[Zee10] Anthony Zee. *Quantum Field Theory in a Nutshell: Second Edition*. In a Nutshell. 41 William Street,Princeton, New Jersey 08540: Princeton University Press, 2010. ISBN: 9781400835324. URL: https://press.princeton.edu/books/ebook/9781400850587/quantum-field-theory-in-a-nutshell.